

Modelling the infrared galaxy evolution using a phenomenological approach

G. Lagache,¹ H. Dole,² J.-L. Puget¹

¹*Institut d'Astrophysique Spatiale, Bât. 121, Université Paris XI, 91405 Orsay Cedex, France*

²*Steward Observatory, University of Arizona, 933 N Cherry Ave, Tucson, AZ, 85721, USA*

Accepted 2002 August 14, Received 2002 June 6

ABSTRACT

To characterise the cosmological evolution of the sources contributing to the infrared extragalactic background, we have developed a phenomenological model that constrains in a simple way the galaxy luminosity function evolution with the redshift, and fits all the existing source counts and redshift distributions, Cosmic Infrared Background intensity and fluctuations observations, from the mid-infrared to the submillimetre range. The model is based on template spectra of starburst and normal galaxies, and on the local infrared luminosity function. Although the Cosmic Infrared Background can be modeled with very different luminosity functions as long as the radiation production with redshift is the right one, the number counts, and the anisotropies of the unresolved background, imply that the luminosity function must change dramatically with redshift, with a rapid evolution of the high-luminosity sources ($L > 3 \times 10^{11} L_{\odot}$) from $z=0$ to $z=1$ which then stay rather constant up to redshift 5. The derived evolution of the IR luminosity function may be linked to a bimodal star formation process, one associated with the quiescent and passive phase of the galaxy evolution and one associated with the starburst phase, triggered by merging and interactions. The latter dominates the infrared and submillimetre output energy of the Universe. The model is intended as a convenient tool to plan further observations, as illustrated through predictions for *Herschel*, *Planck* and *ALMA* observations. Our model predictions for given wavelengths, together with some useful routines, are available for general use.

Key words: galaxies: evolution – infrared: galaxies – galaxies: starburst – galaxies: general – cosmology: observations

1 INTRODUCTION

The discovery of the Cosmic Infrared Background (CIB) (Puget et al. 1996; Fixsen et al. 1998; Hauser et al. 1998; Schlegel et al. 1998; Lagache et al. 1999; Lagache et al. 2000; see Hauser & Dwek 2001 for a review), together with recent deep cosmological surveys in the infrared (IR) and submillimetre (submm) has opened new perspectives on our galaxy formation and evolution understanding. The surprisingly high amount of energy contained in the CIB showed that it is crucial to probe its contributing galaxies to understand when and how the bulk of stars formed in the Universe. Thanks to ISO (Kessler et al., 1996) – mainly at 15 μm with *ISOCAM* (Cesarsky et al. 1996), and 90 and 170 μm with *ISOPHOT* (Lemke et al. 1996) – and ground-based instruments – *SCUBA* (Holland et al. 1998) and *MAMBO* (Bertoldi et al. 2000) at 850 and 1300 μm respectively – deep cosmological surveys have been carried out. It is thus now possible, to various degrees, to resolve the

CIB into discrete sources (e.g. Kawara et al. 1998; Barger et al. 1999; Elbaz et al. 1999; Carilli et al. 2000; Juvela et al. 2000; Linden-Vornle et al. 2000; Matsuhara et al. 2000; Bertoldi et al. 2001; Dole et al. 2001; Elbaz et al. 2002; Scott et al. 2002). The striking result of these surveys concerns the evolution of the IR and submm galaxy population. The source counts are high when compared to no, or moderate, evolution models^{*} for IR galaxies (Guiderdoni et al. 1998; Franceschini et al. 1998). Therefore, it has been necessary to develop new models in the IR. Very recently, several empirical approaches have been proposed to model the high rate of evolution of IR galaxies (e.g. Devriendt & Guiderdoni 2000; Wang & Biermann 2000; Charry & Elbaz 2001; Franceschini et al. 2001; Malkan & Stecker 2001; Pearson 2001; Rowan-Robinson 2001; Takeuchi et al. 2001; Xu et al.

^{*} ‘No-evolution’: the co-moving luminosity function remains equal to the local one at all redshift

2001; Bolland et al. 2002; Wang 2002) which fit all existing source counts, redshift distribution and CIB intensity and fluctuations, although often not all of them. We present in this paper a new model whose preliminary results were published by Dole et al. (2000). The originality of this model was to empirically separate the evolution of the starburst galaxies with respect to the normal galaxies, the current observations implying a strong evolution of the bright part of the Luminosity Function (LF). It was shown for the first time that only the starburst part should evolve very rapidly between $z=0$ and $z=2$, the evolution rate being much higher in the IR than in any other wavelength domain.

We present here a more sophisticated and detailed version of the first model (Dole et al. 2000). Our philosophy is to build the simplest model of the LF evolution, easily deliverable, with the lowest number of parameters but accounting for all observational data. We stress out the point that we include the CIB fluctuations levels as measured by *ISOPHOT* (Lagache & Puget 2000; Matsuhara et al. 2000) and *IRAS* (Miville-Dechénes et al. 2002) as an extra constraint. Recent observations strongly suggest that the bulk of the optical and IR extragalactic background is made of two distinct galaxy populations (see Sect. 2.2). Therefore, we restrict our model in the wavelength domain 10 - 1500 μm , our goal being to quantify the evolution of IR galaxies. The paper is organised as follows: we first summarise our present knowledge on the evolution of IR galaxies, and on the nature of the sources contributing to the Extragalactic Background (Sect. 2). Then, we present the ingredients of the model (Sect. 3). In Sect. 4, we discuss the galaxy templates used in the model. We then present the parametrisation of the local LF (Sect. 5). In Sect. 6 are given the results of the model (evolution of the LF, evolution of the luminosity density, number counts, z -distribution, CIB intensity and fluctuations). And finally the model is used for predictions for the *Herschel* and *Planck* surveys (Sect. 7.2 and 7.3 respectively), gives requirements for future large deep survey experiments (Sect. 7.4) and predictions for *ALMA* observations (Sect. 7.5). A summary is given in Sect. 8.

2 OUR PRESENT KNOWLEDGE

2.1 The strong evolution of IR galaxies: observational evidences

There have been, in the last few years, strong observational evidences indicating extremely high rates of evolution for IR galaxies.

First, galaxy evolution can be observed through its imprint on the far-IR EB (Extragalactic Background). Weakly constrained even as recently as 6 years ago, various observations now measure or give upper/lower limits on the background from the UV to the millimetre (mm) waveband (e.g. Dwek et al. 1998; Gispert et al. 2000; Hauser & Dwek 2001). The data show the existence of a minimum between 3 and 10 μm separating direct stellar radiation from the IR part due to radiation re-emitted by dust. This re-emitted dust radiation contains at least a comparable integrated power as the optical/near-IR, and perhaps as much as 2.5 times

more. This ratio is much larger than what is measured locally ($\sim 30\%$). The CIB is thus likely to be dominated by a population of strongly evolving redshifted IR galaxies. Since the long wavelength spectrum of the background is significantly flatter than the spectrum of local star-forming galaxies, it strongly constrains the far-IR radiation production rate history (Gispert et al. 2000). The energy density must increase by a factor larger than 10 between the present time and a redshift $\sim 1-2$ and then stay rather constant at higher redshift (till ~ 3), contrary to the ultraviolet radiation production rate which decreases rapidly.

Second, several deep cosmological surveys at 15, 90, 170, 850 and 1300 μm have resolved a fraction of the CIB into discrete sources. For all surveys, number counts indicate a very strong cosmological evolution of IR galaxies, in total power radiated but also in the shape of the LF. This is particularly obvious at submm wavelengths where the EB is dominated by high luminosity galaxies (see the *SCUBA* and *MAMBO* results). The high rates of evolution exceed those measured in other wavelength domain as well as those observed for quasars and Active Galactic Nuclei (AGNs).

Finally, high rates of evolution are suggested by the detection of the CIB Poissonian fluctuations at a high level at 60 and 100 μm with *IRAS* (Miville-Dechénes et al., 2002) and 170 μm with *ISOPHOT* (Lagache & Puget 2000; Matsuhara et al. 2000). For example, Matsuhara et al. (2000) give the constraints on the galaxy number counts down to 35 mJy at 90 μm and 60 mJy at 170 μm , which indicate the existence of a strong evolution down to these fluxes in the counts.

2.2 Sources making the Extragalactic Background

2.2.1 Optical versus IR and submm EB sources

Recent observations show that the bulk of the optical and IR EB is made by two distinct galaxy populations (e.g. Aussel et al. 1999). Therefore, one of the key question is whether the dusty star forming galaxies are recognizable from optical/near-IR data alone.

In the local Universe, Sanders & Mirabel (1996) show that the bolometric luminosity of IR galaxies is uncorrelated with optical spectra. The color excess derived from the Balmer lines ratio does not significantly depend on the IR luminosity, IR color or optical spectral type (Veilleux et al. 1999). In fact, neither the moderate strength of the heavily extinguished starburst emission lines, nor their optical colors can distinguish them from galaxies with more modest rates of star formation (Elbaz et al. 1999; Trentham et al. 1999; Poggianti et al. 1999). However, recently, Poggianti & Wu (2000) and Poggianti et al. (2001) show that the incidence of $e(a)^\dagger$ sources in the different IR selected samples seems to suggest that the $e(a)$ signature might be capable of identifying from optical data alone a population of heavily

[†] Galaxies with strong Balmer absorption lines and [OII] in emission (Poggianti & Wu (2000) and references therein)

extinct starburst galaxies. Reproducing the e(a) spectrum requires the youngest stellar generations to be significantly more extinguished by dust than older stellar populations, and implies a strong ongoing star formation activity at a level higher than in quiescent spirals.

At intermediate redshift ($0.3 < z < 1$), one of the main information on IR galaxies comes from identifications of *ISOCAM* deep fields. For example, Flores et al. (1999a,b) presented results of a deep survey of one of the CFRS fields at 6.75 and 15 μm . At 15 μm , most (71%) of the sources with optical spectroscopy are classified as e(a) galaxies. The FIR luminosities of the Flores et al. e(a) galaxies are between $5.7 \cdot 10^{10}$ and $2 \cdot 10^{12} L_{\odot}$. This is the first confirmation of the IR luminous nature of e(a) galaxies. More recently, Rigopoulou et al. (2000) using VLT spectroscopy found that optical *ISOCAM* counterparts in the HDF-south are indistinguishable from the dusty luminous e(a) galaxies.

All these studies at low and intermediate redshift seem to show that IR galaxies predominantly exhibit e(a) signatures in their optical spectra. On the contrary, in optically selected surveys of field galaxies, e(a) spectra are present but seems to be scarce (less than 10%, see for example Poggianti et al. 1999). In fact evidence for high e(a) incidences are found in merging or interacting systems or active compact groups. A complete study of the IR emission of e(a) galaxies is still to be done.

At much higher redshift, there are other evidences that the optically selected samples and bright IR samples (e.g. the SCUBA blank field sample) are different. For example, Chapman et al. (2000) have performed submm photometry for a sample of Lyman Break galaxies whose UV properties imply high star formation rates. They found that the integrated signal from their Lyman break sample is undetected in the submm. This implies that the population of Lyman break galaxies does not constitute a large part of the detected blank field bright submm sources.

In conclusion, it is clear that the optical and IR EBs are not dominated by the same population of galaxies. Therefore, we restrict our model in the wavelength domain 10-2000 μm , our goal being to quantify the evolution of the IR galaxies.

2.2.2 The CIB sources

In the HDF-N field (HST Deep Field North), Aussel et al. (1999) and Elbaz et al. (1999) find that 30 to 50 % of *ISOCAM* galaxies are associated with optical sources showing complexe structures and morphological peculiarities. Moreover, Cohen et al. (2000) show, in the HDF-N, that more than 90% of the faint *ISOCAM* sources are members of concentrations. This shows that past or present interactions or merging play a large role in triggering the IR emission of galaxies. All the studies of *ISOCAM* field sources show that the bulk of the CIB at 15 μm comes from galaxies which have bolometric luminosities of about 10^{11} - $10^{12} L_{\odot}$, high masses ($\sim 10^{11} M_{\odot}$) and redshift between 0.5 and 2. They experience an intense stellar formation ($100 M_{\odot}/\text{yr}$) which appears to be uncorrelated with the faint blue galaxy pop-

ulation dominating the optical counts at $z \sim 0.7$ (Ellis 1997; Elbaz et al. 1999). In galaxy clusters all *ISOCAM* sources are found preferably at the periphery where there is still some star formation (Biviano et al. 1999).

At longer wavelengths, source identifications are much more difficult. Thus, characterising the nature of the galaxies is a long time process. However, we already have some indications. The *FIRBACK* survey at 170 μm detected about 200 galaxies (Dole et al. 2001) making less than 10% of the CIB. Schematically *FIRBACK* sources comprise 2 populations: one cold and nearby ($L \sim 10^9 - 10^{11} L_{\odot}$) and one cold or warm very luminous ($L \sim 10^{12} L_{\odot}$) with redshift lower than 1.2. The optical spectroscopy of the brightest *FIRBACK* sources reveals an ‘*IRAS*-like’ starburst nature (Dennefeld et al. in prep; Patris et al. 2002) with a moderate star-formation rate ($10 M_{\odot}/\text{yr}$). These results are very similar to those of Kakazu et al. (2002) who found that 62% of the Lockman Hole 170 μm sources are at redshift below 0.3 with luminosities lower than $10^{12} L_{\odot}$ (based on Arp220 spectrum), the rest being mostly ultraluminous IR galaxies with redshift between 0.3 and 1. In their sample, the 170 μm sources appear also to be powered primarily by star formation.

In the submm, the main indication comes from the *SCUBA* deep surveys (e.g. Hughes et al. 1998; Barger et al. 1999; Eales et al. 1999; Scott et al. 2002). These surveys suggest that faint 850 μm sources are mostly ultraluminous galaxies at typical redshift between 1 and 4 (e.g. Eales et al. 2000). *SCUBA* sources above 3 mJy account for 20-30 % of the EB at 850 μm . The present data show that the bulk of the submm EB is likely to reside in sources with 850 μm fluxes near 0.5 mJy. Barger et al. (1999) estimate that the FIR luminosity of a characteristic 1 mJy source is in the range $4\text{-}5 \cdot 10^{11} L_{\odot}$, which is also the typical luminosities of sources making the bulk of the CIB at 15 μm . Moreover, as for the 15 μm sources, several groups have suggested that the submm sources are associated with merger events (e.g. Smail et al. 1998; Lilly et al. 1999). All these results show that the integrated power of the LF at redshift greater than ~ 0.5 must be dominated by sources with luminosities of a few $10^{11} L_{\odot}$ while the local LF is dominated by sources with luminosities of the order of $5 \cdot 10^{10} L_{\odot}$.

2.2.3 The AGN contribution to the IR output energy

At low- z , Veilleux et al. (1999) and Lutz et al. (1999) show that most of the IR sources are powered by starbursts. The AGN contribution appears dominant only at very high luminosities ($L > 2 \cdot 10^{12} L_{\odot}$). Also using *FIRBACK* nearby bright source spectroscopy, we find that less than 10% of sources show AGN signs (Dennefeld et al., in prep; Patris et al. 2002). The same conclusions are reached by Kakazu et al. (2002). At intermediate z , from optical and X-rays studies of *ISOCAM* sources making the bulk of the CIB, several groups show that 15 μm sources are mostly starburst galaxies (e.g. Fadda et al. 2002). At much higher z , the main indication comes from X-ray observations of *SCUBA* sources (Barger et al. 2001; Fabian et al. 2000; Hornschemeier et al. 2000; Severgnini et al. 2000). All these observations of submm galaxies in the X-rays are consistent with starburst-dominated emission. However, recently, Page et al. (2002)

present a result of *SCUBA* observations of eight X-ray absorbed active galactic nuclei from $z=1$ to $z=2.8$ and find, for half of them, a $850\ \mu\text{m}$ submm counterpart. Nevertheless, the high $850\ \mu\text{m}$ fluxes (greater than 5.9 mJy) suggest that these sources are hyperluminous galaxies. Such galaxies do not dominate the IR output of the Universe.

Considering the whole CIB energy budget, and based on the assumptions that 10% of the mass accreting into black hole is turned into energy and that the black hole masses measured in the HDF (Ford et al. 1998) are typical of galaxies, the AGN background energy would be at the order of 10% of that from stars (Eales et al. 1999). These calculations are highly uncertain but are supported by the work of Almaini et al. (1999). And recently, more direct evidences have been obtained. For example, Severgnini et al. (2000) show that the 2-10 keV sources making at least 75% of the X-ray background in this band contribute for less than 7% to the submm background.

On the modelisation side, several groups (e.g. Xu et al. 2001; Rowan-Robinson 2001) show that the starburst galaxy evolves much more rapidly than the AGN-dominated sources, making the AGN contribution to the CIB relatively small.

In conclusion, it is clear that AGNs do not dominate the IR output energy of the Universe. Therefore, we will consider hereafter that IR galaxies are mostly powered by star formation and we use Spectral Energy Distributions (SED) typical of these star-forming galaxies. The differences in SED for the small fraction of AGN dominated IR galaxies would not affect significantly the results of our model which is built with only two galaxy populations ('normal' and starburst) defined by their SEDs.

3 INGREDIENTS OF THE MODEL

At a given wavelength $\lambda=\lambda_0$, the flux S_ν of a source at redshift z , as a function of the rest-frame luminosity L_ν (in W/Hz) can be written:

$$S_\nu(L, z, \lambda = \lambda_0) = \frac{(1+z) \times K(L, z) \times L_\nu(L, \lambda = \lambda_0)}{4\pi D_L^2} \quad (1)$$

where D_L is the luminosity distance and $K(L, z)$ is the K-correction factor defined as :

$$K(L, z) = \frac{L_{\nu(1+z)}}{L_{\nu(z=0)}} \quad (2)$$

This correction is specific of the spectrum of the considered population at given L and z . In practice, the rest-frame luminosity L_ν is convolved by the band pass filter centred on $\lambda=\lambda_0$. The number of sources per solid angle and redshift interval is:

$$\frac{dN}{dz d\text{Log} L}(L, z) = N_0(L, z) \times (1+z)^3 \times \frac{dV}{dz} \quad (3)$$

where dV/dz is the differential volume element fixed by the cosmology and N_0 is the number of sources per unit volume and luminosity interval as a function of redshift. N_0 is given by the LF.

The differential counts at a given flux S and wavelength $\lambda=\lambda_0$ write as:

$$\frac{dN}{dS} = \int_L \int_z \frac{dN}{dz d\text{Log} L}(L, z) \times \frac{dz}{dS}(L, z) \times d\text{Log} L \quad (4)$$

We then obtain the integral counts:

$$N(> S) = \int \frac{dN}{dS} dS \quad (5)$$

the CIB intensity produced by all sources with $S < S_{max}$:

$$I_{CIB} = \int_0^{S_{max}} S \frac{dN}{dS} dS \quad (6)$$

and the CIB intensity fluctuations (the shot noise) from sources below a given detection limit S_0 (that could correspond to either the confusion or the sensitivity limit) measured by the level of the white noise power spectrum:

$$P_{fluc} = \int_0^{S_0} S^2 \frac{dN}{dS} dS \quad \text{Jy}^2/\text{sr} \quad (7)$$

We build the simplest model with the lowest number of parameters and ingredients which fits all the observations. We first fix the cosmology ($\Omega_\Lambda=0.7$, $\Omega_0=0.3$ and $h=0.65$) from the combination of the most recent CMB anisotropy measurements (e.g. de Bernardis et al. 2002) the distance-luminosity relation of type Ia supernovae (e.g. Perlmutter et al. 1999) and the measure of galaxy distances using Cepheids (e.g. Freedman et al. 2001). We then construct the 'normal' and starburst template spectra : at each population and luminosity is associated one spectrum (see Sect. 4). We finally search for the best evolution of the LF (Eq. 3) that reproduces the number counts (Eq. 4-5), the CIB and its fluctuations (Eq. 6 and 7 respectively), assuming that the LF evolution is represented by the independent evolution of the two populations. A rather remarkable result, as will be seen later, is that two populations only can fit all the data.

4 BUILDING GALAXY TEMPLATES

4.1 Starburst galaxies

The luminous IR starburst galaxies emit more than 95% of their energy in the far-IR. Spectra of such galaxies have been modeled by Maffei (1994), using the Désert et al. (1990) dust emission model and the observationnal correlation for the *IRAS* Bright Galaxy Sample of the flux ratio 12/60, 25/60 and 60/100 with the IR luminosity (Soifer & Neugebauer, 1991). We start from this model and modify it slightly to better take into account recent observationnal constraints. The significant improvements are the following:

- First we replace the Désert et al. (1990) PAHs template by the Dale et al. (2001) one, keeping the same amount of energy in the mid-IR.
- We slightly modify the spectral shape in the near and mid-IR: we increase the PAH and Very Small Grains proportions (by a factor ~ 2) but add some extinction, slowly increasing with the luminosity.
- Finally, we broaden the far-IR peak (also a continuous change with the luminosity) and flattens slightly the long wavelength spectrum (Dunne et al. 2000; Dunne & Eales 2001; Klaas et al. 2001).

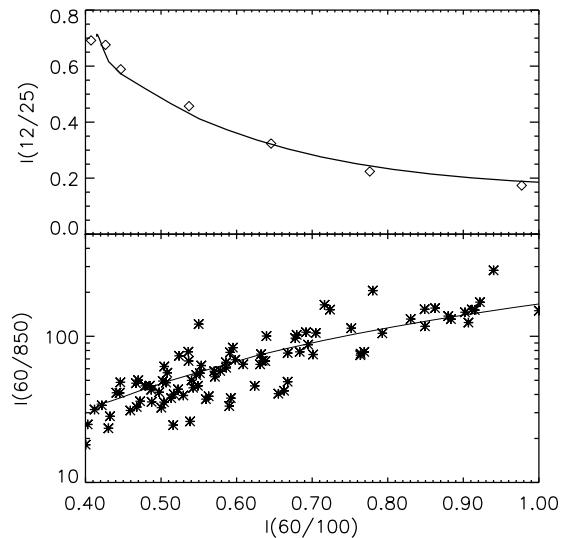


Figure 1. Color diagrams from the model (continuous lines), compared with Soifer & Neugebauer 1991 (diamonds) and Dunne et al. 2000 (stars) data points.

Fig. 1 shows the (12/25, 60/100) and (60/850, 60/100) color diagrams compared with Soifer & Neugebauer (1991) and Dunne et al. (2000) observations. We see a very good agreement between the templates and observations. The average luminosity spectra sequence is shown on Fig. 2. For the ‘normal’ starbursting galaxies ($L_{IR} < 10^{11} L_{\odot}$), we also check that the 7/15 versus 60/100 diagram was in good agreement with Dale et al. (2001).

Such a representation of galaxy SEDs that assigns only one spectrum per luminosity does not take into account the dispersion of the colors (e.g. the 60/100 ratio) observed for a given luminosity (as in Xu et al. 2001 or Chapman et al. 2002a). However, we do not have enough measured colors to do a statistical analysis of their variations with the luminosities. The only colors measured for a large sample are the IRAS colors (principally the 60/100). Using only the 60/100 color as a tracer of the dispersion for a given luminosity, may not improve the representation as for example two very different long-wavelength spectra can have the same 60/100 color (e.g. NGC 7821 and NGC 0549, Stickel et al. 2000).

4.2 Normal spiral galaxies

For the ‘normal’ galaxies (i.e. standard IR counterparts of spiral galaxies with more than half of their energy output in the optical), we take an unique spectrum derived mainly from the *ISOPHOT* serendipity survey (Stickel et al. 2000) and the nearby *FIRBACK* galaxy SEDs, together with longer wavelength data from Dunne et al. (2000) and Dunne & Eales (2001).

The *ISOPHOT* serendipity survey has revealed a population of nearby cold galaxies (Stickel et al. 1998, 2000), under-represented in the 60 μ m *IRAS* sample. The distribution of I_{170}/I_{100} flux ratio shows that about half of the galaxies have a flux ratio between 1 and 1.5, indicating that

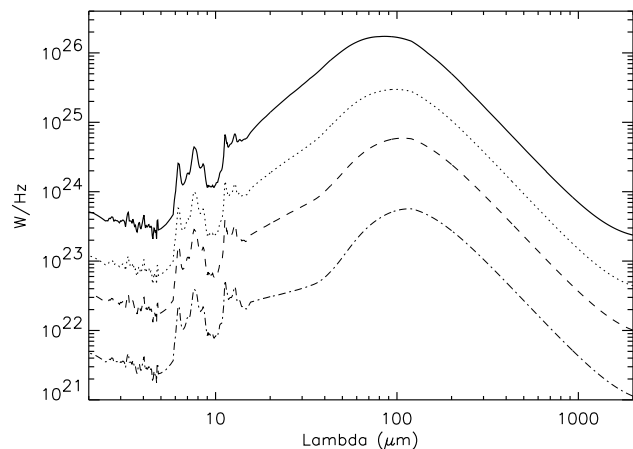


Figure 2. Starburst model spectra for different luminosities: $L=3 \cdot 10^{12} L_{\odot}$ (continuous line), $L=5 \cdot 10^{11} L_{\odot}$ (dotted line), $L=10^{11} L_{\odot}$ (dashed line) and $L=10^{10} L_{\odot}$ (dotted-dashed line)

the FIR spectra are mostly flat between 100 and 200 μ m. Very few show a downward trend in this wavelength range, this trend being typical of warm starburst galaxies (see Fig. 2). Most important is the large fraction of sources (more than 40 %) which have $I_{170}/I_{100} > 1.5$, indicating a rising spectrum beyond 100 μ m similar to that seen for example in the Milky Way galactic ridge, a property known for more than 20 years from early balloon-borne measurements (Serra et al. 1978, Silverberg et al. 1978).

In the *FIRBACK* N1 field (Dennefeld et al., in prep), the brightest sources show mean IR color similar to that of Stickel et al. (2000): $I_{170}/I_{100} \sim 1.3$ and $I_{60}/I_{100} \sim 0.47$. These objects are often associated with bright optical spiral galaxies (e.g. Fig. 3) with also typical 15 μ m fluxes such as $I_{170}/I_{15} \sim 42$. Finally recent observations at 450 μ m (Dunne & Eales 2000) reveal also the presence, in normal galaxies, of a colder component than previously thought.

Therefore, we take for the normal galaxy the ‘cold’ template presented in Fig 4. This template have mean IR color of $I_{170}/I_{100} = 1.42$, $I_{60}/I_{100} = 0.35$, $I_{170}/I_{15} = 45$ and $I_{100}/I_{850} = 77$. For the Mid-IR part of the template, we use the spectral signature that applies to the majority of star-forming galaxy presented in Helou (2000). More observations around the maximum intensity (~ 100 -200 μ m) and in the submm are needed if we want to refine the template and describe its variations with the luminosity.

Note that we do not make any evolution of the ‘normal’ and starburst template spectra with the redshift. As shown in Chapman et al. (2002a), the available data for high redshift, far-IR galaxies do not reveal evidence for any strong evolution in the characteristic temperature of the color distribution over $0 < z < 3$. We can also test this hypothesis of ‘no-evolution’ using the two high-redshift sources N1-040 and N1-064 detected in the *FIRBACK* N1 field (Chapman et al. 2002b). For these two sources, we do a blind search for both the luminosity and redshift using our template spectra, based on a χ^2 test. For N1-064 the ‘normal’ and starburst template gives the same χ^2 with $\text{Log}(L)=12.2$ and $z=0.5$ and

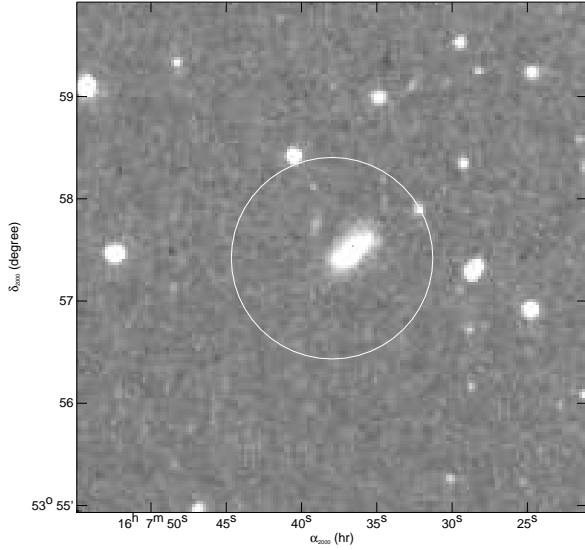


Figure 3. Example of association of one bright *FIRBACK* 170 μm source with a “cold” spiral galaxy (the optical image is from the DSS; the white circle corresponds to the 170 μm error position). IR color ratios for this source are $I_{60}/I_{100}=0.6$, $I_{170}/I_{100}=1.4$ and $I_{170}/I_{15}=51$

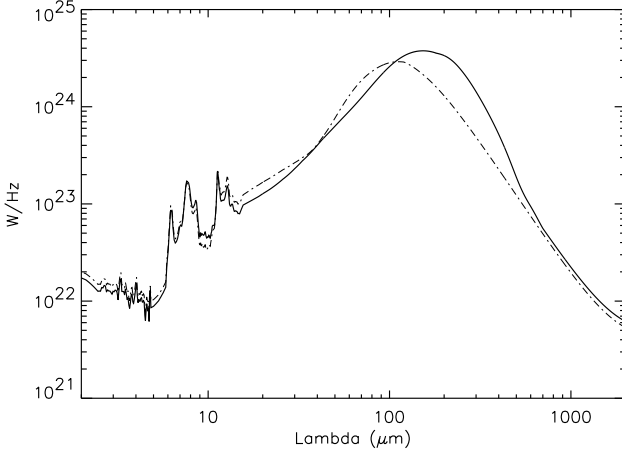


Figure 4. Template spectrum for the normal galaxies (continuous line), compared with the template spectrum for the starburst galaxies (dash-dot line), for the same luminosity $L=5 \times 10^{10} L_{\odot}$

$\text{Log}(L)=12.8$ and $z=1.05$ respectively. The starburst template gives results in good agreement with Chapman et al. (2002b). For N1-040, the best χ^2 is obtained for the ‘normal’ template with $\text{Log}(L) = 12.2$ and $z=0.45$, which is in perfect agreement with Chapman et al. (2002b). The template spectra give photometric redshifts in good agreement with the spectroscopic redshifts, suggesting no strong evolution of the galaxy SEDs over $0 < z < 1$.

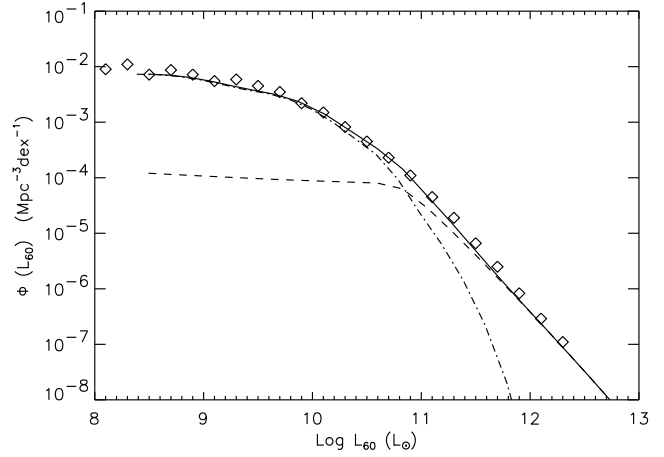


Figure 5. Luminosity function at 60 μm (model: normal galaxies: dot-dash line, starburst galaxies: dash line, total: continuous line) compared with Saunders et al. 1990 (squares).

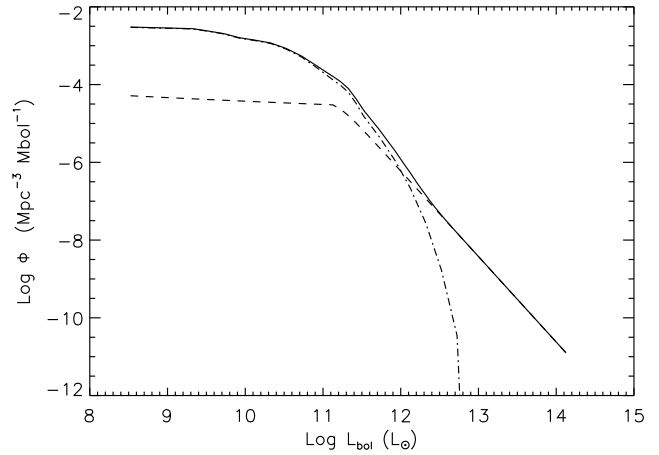


Figure 6. Bolometric luminosity function at $z=0$ (normal galaxies: dot-dash, starburst galaxies: dash and total: continuous)

5 PARAMETRISATION OF THE LOCAL LUMINOSITY FUNCTION

A detailed comparison of the luminosity function of IR bright galaxies with other classes of extragalactic objects has been done in Sanders & Mirabel (1996). The most striking results are (i) the high luminosity tail of the IR galaxy LF is clearly in excess of what expected from a Schechter function and (ii) at luminosities below $\sim 10^{11} L_{\odot}$, the majority of optically selected objects are relatively weak far-IR emitters (as shown by *IRAS*, *ISOPHOT* and *SCUBA* observations). Accordingly, we decompose the IR LF in two parts: (1) the ‘low-luminosity’ part (dominated by normal galaxies) that follows the shape of the optical LF and (2) the ‘high-luminosity’ part dominated by starburst galaxies (note however that each part covers the whole range of luminosities).

We start from the local LF at 60 μm from Saunders et al. (1990) (Fig. 5). We convert the 60 μm LF in a bolometric LF ($L=1\text{--}1000 \mu\text{m}$) using our template spectra: at the 'low-luminosity' and 'high-luminosity' part, we assign the 'normal' and starburst template spectra respectively[‡]. The bolometric LF (1-1000 μm) used in the model is shown in Fig. 6.

The parametrisation and redshift evolution of the two parts of the bolometric LF is done using the following:

- For the normal galaxies:
 - A LF at $z=0$ parametrised by an exponential with a cutoff in luminosity L_{cutoff} :

$$\Phi_{\text{normal}}(L) = \Phi_{\text{bol}}(L) \times \exp\left(\frac{-L}{L_{\text{cutoff}}}\right) \quad (8)$$

- A weak number evolution
- For the starburst galaxies:
 - A LF described by:

$$\Phi_{SB}(L, z) = \Phi_{\text{bol}}(L = 2.5 \cdot 10^{11} L_{\odot}) \quad (9)$$

$$\times \left(\frac{L}{2.5 \cdot 10^{11} L_{\odot}}\right)^{SB_{\text{slope}}} \times \exp\left(-\frac{L_{\text{knee}}(z)}{L}\right)^3$$

- An evolution of the luminosity of the knee (L_{knee}) with the redshift
- A constant slope of the LF at high luminosities (SB_{slope}), not redshift dependent
- An evolution of the luminosity density with the redshift, $\varphi(z)$, that drives the LF evolution:

$$\Phi_{SB}(L, z) = \Phi_{SB}(L, z=0) \times \left(\frac{\varphi(z)}{\varphi(z=0)}\right) \quad (10)$$

- An integrated energy at $z=0$ as observed: $SB_{\text{norm}} = \varphi(z=0)$

6 RESULTS AND DISCUSSIONS

6.1 LF evolution derived from observations

Although the number of parametres is quite low, it is too much time consuming to do a blind search through the whole parametre space. We therefore search the best solution for the parametres near values expected from direct observational evidences:

- We fix the normal galaxy evolution (passive evolution) such as it nearly follows the number density evolution of optical counts up to $z=0.4$:

$$\Phi_{\text{normal}}(L, z) = \Phi_{\text{normal}}(L, z=0) \times (1+z).$$

We arbitrarily stop the evolution at $z=0.4$ and keep this population constant up to $z=5$ and then let the population decreases up to $z=8$ (see Fig. 8)

[‡] We have also checked the validity of the long-wavelength part of our template spectra by comparing the 850 μm LF with Dunne et al. (2000)

- An estimate of L_{knee} is given by deep surveys at 15 and 850 μm : the bulk of the CIB at 15 μm and 850 μm is made by galaxies with $L \sim 1\text{--}5 \cdot 10^{11} L_{\odot}$ (e.g. Barger et al. 1999; Elbaz et al. 2002)

- We have indications on the evolution of the luminosity density, $\varphi(z)$, for the starburst galaxies, directly inferred from the CIB spectrum shape by Gispert et al. (2000) which is used as a starting point to adjust the model.

- We take $SB_{\text{norm}} = 10^7 L_{\odot}/\text{Mpc}^3$ which is roughly the value observed locally.

- We take $SB_{\text{slope}} = -2.2$ (Kim & Sanders, 1998)

The best evolution of the LF that reproduces IR number counts, redshift distributions and CIB observations is shown on Fig. 7. It is obtained with:

- $L_{\text{cutoff}} = 5 \cdot 10^{11} L_{\odot}$
- $L_{\text{knee}}(z) = 8 \cdot 10^{10} \times (1+z)^3 L_{\odot}$ up to $z=1.5$ and then $L_{\text{knee}}(z) = L_{\text{knee}}(z=1.5)$.

Moreover, to avoid a 'break' in the evolved luminosity function (as in Dole et al. 2000), we modify the low-luminosity part of the starburst LF with the redshift (up to $z=5$) according to:

$$\Phi_{SB}(L, z) = \Phi_{SB}(L = L_{\text{max}}, z) \times \left(\frac{L_{\text{max}}}{L}\right)^{(1+z)^2} \quad (11)$$

where L_{max} is the luminosity corresponding to the maximum of $\Phi_{SB}(L, z)$.

We see a very high rate of evolution of the starburst part which peaks at $z \sim 0.7$ (Fig. 8) and then remains nearly constant up to $z=4$ (as shown for example by Charry & Elbaz, 2001). We compare on Fig. 8 the co-moving luminosity density distribution as derived from the model with the Gispert et al. (2000) one. There is a good overall agreement. However, the model is systematically lower than the Gispert et al. (2000) determination for redshifts between 0.5 and 2. This comes from the fact that the CIB values at 100 and 140 μm used in Gispert et al. (2000) were slightly overestimated (Renault et al. 2001) leading in an overestimate of the luminosity density distribution at low redshift.

6.2 Comparison model-observations

6.2.1 The number counts

Fig. 9 shows the comparison of the number counts at 15 μm (Elbaz et al. 1999), 60 μm (Hacking & Houck 1987; Gregorich et al. 1995; Bertin et al. 1997; Lonsdale et al. 1990; Saunders et al. 1990; Rowan-Robinson et al. 1990), 170 μm (Dole et al. 2001) and 850 μm (Smail et al. 1997; Hughes et al. 1998; Barger et al. 1999; Blain et al. 1999; Borys et al. 2002; Scott et al. 2002; Webb et al. 2002) with the observations. We have a very good overall agreement (we also agree with the 90 μm number counts of Serjeant et al. 2001 and Linden-Vornle et al. 2001).

6.2.2 The redshift distributions: Need for a normal ‘cold’ population

On Fig. 10 is shown the redshift distribution of resolved sources at 15, 60, 170 and 850 μm . The 15 μm redshift distribution is in very good agreement with that observed by Flores et al. (1999b) and Aussel et al. (1999). At 850 μm , we predict that most of the detected sources are at $z > 2.5$. At 170 μm , we predict that about 62% of sources with fluxes $S > 180$ mJy (4σ in Dole et al. 2001) are at redshift below 0.25, the rest being mostly at redshift between 0.8 and 1.2. We know from the *FIRBACK* observations that the redshift distribution predicted by the model is very close to that observed at 170 μm : it is clear from these observations that we have a bi-modal z -distribution (Sajina et al. 2002; Denefeld et al. in prep). Moreover, very recently, Kakazu et al. (2002) published first results from optical spectroscopy of 170 μm Lockman Hole sources. They find that 62% of sources are at $z < 0.3$ with IR luminosities (derived using Arp220 SED) lower than $10^{12} L_{\odot}$, the rest being at redshift between 0.3 and 1, which is in very good agreement with the model prediction. It is very important to note that the agreement between the model and observations can only be obtained with the local ‘cold’ population. A model containing only starburst-like template spectra and ‘warm’ normal galaxies overpredicts by a large factor the peak at $z \sim 1$ (as in Charry & Elbaz 2001 for example).

6.2.3 The CIB and its anisotropies

The predicted CIB intensity at specific wavelengths, together with the comparison with present observations are presented in Table 2 and in Fig. 11. We have a very good agreement with the estimates at 60 μm (Miville-Deschênes et al. 2002), 100 μm (Renault et al. 2001), and 170 μm (Kiss et al. 2001) and the *FIRAS* determinations (Fixsen et al. 1998; Lagache et al. 2000). We are also in good agreement with the lower limit derived from 15 μm counts (Elbaz et al. 2002), combined with the upper limit deduced from high energy gamma-ray emission of the active galactic nucleus Mkn 501 (Renault et al. 2001). According to the model, sources above 1 mJy at 850 μm contribute for about 30% of the CIB. At 15 μm , with the deepest *ISOCAM* observations (Altieri et al. 1999; Aussel et al. 1999; Metcalfe 2000) about 70 % of the CIB has been resolved into individual sources.

Finally, we compare the model predictions for the CIB fluctuations with the present observations at 60, 90, 100 and 170 μm (Table 3). For the comparison we need to remove the contribution of the brightest sources that make the bulk of the fluctuations (sources with fluxes $S > S_{max}$). When S_{max} is quite high (at the order of 500 mJy - 2 Jy), the fluctuations are dominated by the strongest sources, making the result very dependent on the accuracy of the evaluation of S_{max} . This is why the comparison observations/model is very difficult[§]. For S_{max} around 50-150 mJy, the fluctuations are dominated by the faint and numerous sources that dominate the CIB and the values do not depend critically on

the exact value of S_{max} . We see from Table 3 that although for some observations the model can be lower or greater by factor 1.5 in amplitude, we have an overall very good agreement. We stress out that reproducing the CIB fluctuations gives strong constraints on the LF evolution. For example, evolution such that we better reproduce the 850 μm counts gives too high CIB fluctuations. Future observations with better accuracy will show if these minor discrepancies disappear or are indicative that the bright submm counts are overestimated due to a high fraction of gravitationally lensed sources (Perrotta et al. 2002), or are simply indicative that the present phenomenological model is too simple ! The level of the predicted CIB fluctuations for dedicated experiments (as for example *Boomerang* or *Maxima*), with respect to the cirrus confusion noise and instrumental noise will be discussed in detail in Piat et al. (in prep).

At 170 μm , it is clear from Fig. 12 that the redshift distributions of sources that are making the CIB and those making the bulk of the fluctuations are similar. The fluctuations are not dominated by bright sources just below the detection threshold but by numerous sources at higher redshift. Thus, in this case, studying the CIB fluctuations gives strong constraints on the CIB source population. This is true in the whole submm-mm range. The population of galaxies, where the CIB peaks, will not be accessible by direct detection in the coming years. For example, *SIRTF* will resolve about 20% of the background at 160 μm (Dole et al. 2002), *PACS* about 50 % at 170 μm (Sect. 7.2.2) and *SPIRE* less than 10% at 350 μm (Sect. 7.2.1).

In conclusion, we have seen that our model gives number counts, redshift distributions, CIB intensity and fluctuations that reproduce all the present observations. It can be now used for future experiment predictions, in particular for *Herschel*, *Planck* and *ALMA* observations. For *SIRTF*, a complete and more detailed study, including simulations and a detailed discussion on the confusion, is done in Dole et al. (2002).

7 PREDICTIONS FOR FUTURE EXPERIMENTS

7.1 The confusion noise from extragalactic sources

The confusion noise[¶] is usually defined as the fluctuations of the background sky brightness below which sources cannot be detected individually. These fluctuations are caused by intrinsically discrete extragalactic sources. In the far-IR, submm and mm wavelengths, due to the limited size of the telescopes compared to the wavelength, the confusion noise play an important role in the total noise budget. In fact, the confusion noise is often greater than the instrumental noise, and is thus limiting severely the surveys depth. The total variance σ^2 of a measurement within a beam due to extragalactic sources with fluxes less than S_{lim} is given by:

[§] We cannot compare the model predictions with the Kiss et al. (2001) results since we have no information on S_{max}

[¶] We only consider the confusion noise due to extragalactic sources since, in the high galactic latitude cosmological fields, the cirrus confusion noise is negligible.

$$\sigma^2 = \int f^2(\theta, \phi) d\theta d\phi \int_0^{S_{lim}} S^2 \frac{dN}{dS} dS \quad (12)$$

where $f(\theta, \phi)$ is the two-dimensional beam profile (in steradians), S the flux in Jy, and $\frac{dN}{dS}$ the differential number counts in $\text{Jy}^{-1} \text{sr}^{-1}$. We call S_{lim} the confusion limit.

The confusion noise can be determined using two criteria: the so-called photometric and source density criteria (see Dole et al. 2002 for a full description). The photometric criterion is related to the quality of the photometry of detected sources, the flux measured near S_{lim} being severely affected by the presence of fainter sources in the beam. It is defined by the implicit equation:

$$S_{lim} = q_{phot} \times \sigma(S_{lim}) \quad (13)$$

where q_{phot} measures the photometric accuracy and is usually taken between 3 and 5.

The source density criterion is related to the completeness of detected sources above S_{lim} directly related to the probability to lose sources too close to each other to be separated. There is a threshold above which the density of sources above S_{lim} is such that a significant fraction of the sources is lost (it is impossible to separate the individual sources anymore). For a given source density (with a Poissonian distribution) $N(>S)$, corresponding to a flux limit S_{lim} , the probability P to have the nearest source with flux greater than S_{lim} located closer than the distance θ_{min} is:

$$P(<\theta_{min}) = 1 - e^{-\pi N \theta_{min}^2} \quad (14)$$

θ_{min} is the distance below which sources cannot be separated and is a function of the beam profile. If we note θ_{FW} , the FWHM of the beam profile, θ_{min} can conveniently be expressed in unity of θ_{FW} , $\theta_{min} = k \times \theta_{FW}$. As an illustration, simulations of source extraction at the *MIPS/SIRTF* wavelengths show that $k=0.8$ should be achievable (Dole et al. 2002). Therefore, in the following, we fix $k=0.8$. We choose the maximum acceptable probability of not being able to separate the nearest source $P_{max} = 0.1$. In this case, the source density is equal to $1 / 17.3\Omega$ (Table 1) and the corresponding most probable distance is about $1.7 \times \theta_{FW}$. Using Eq. 14, we can derive $N(>S)$ and thus find the corresponding S_{lim} . Then, using Eq. 12, we compute σ . The source density criterion leads to a value of an equivalent $q_{density} = \frac{S_{lim}}{\sigma}$. If $q_{density}$ is greater than standard values of q_{phot} (3 to 5), then the confusion noise is given by the source density criterion. If not, then the photometric criterion has to be used to derive the confusion noise. The classical confusion limit of 1 source per 30 beams corresponds to $k=1$ and $P \sim 0.1$. Nevertheless it can still lead to mediocre photometry for very steep $\log N$ - $\log S$.

The transition between the photometric and source density criterion is around $200 \mu\text{m}$, depending on telescope diameters. For example for *SIRTF*, at 24 and $70 \mu\text{m}$, the source density criterion gives $q_{density} \sim 7$ (Dole et al. 2002). In this case, the source density criterion has to be used to derive the source confusion and it leads to a very good photometric quality. On the contrary, at the *Planck* wavelengths, the source density criterion gives $q_{density} \sim 1$, leading the source detection limited by the photometric quality. Furthermore,

Table 1. Number of beams per sources for different probability P to have the nearest source located closer than the distance $\theta_{min} = k \times \theta_{FW}$ with $\theta_{FW}^2 \sim \Omega/1.1$ (valid for both Gaussian and Airy disk beams).

	$P = 0.05$	$P = 0.1$	$P = 0.15$
$k=0.8$	35.6	17.3	11.2
$k=0.9$	45.1	22.0	14.2
$k=1.0$	55.7	27.1	17.6

this illustrates the limits of doing high signal-to-noise observations ‘to beat the confusion’.

In the following, we derive the confusion noise for future long wavelength dedicated surveys. We assume that the sources are randomly distributed on the sky. The effect of the clustering on the confusion noise will be investigated by Blaizot et al. (in prep) using the hybrid model described in Guiderdoni et al. (2001) and Hatton et al. (2002). The number counts at long wavelengths derived from the model and usefull for the following predictions are shown on Fig. 13.

7.2 The *Herschel* deep surveys

The ‘*Herschel* Space Observatory’ (Pilbratt, 2001) is the fourth cornerstone mission in the European Space Agency science programme. It will perform imaging photometry and spectroscopy in the far-IR and submm part of the spectrum, covering approximately the $60\text{--}670 \mu\text{m}$ range. *Herschel* will carry a 3.5 metre diameter passively cooled telescope. Three instruments share the focal plane: two cameras/medium resolution spectrometres, *PACS* and *SPIRE*, and a very high resolution heterodyne spectrometre, *HIFI*.

In Table 4 are shown the confusion noises and limits at *PACS* and *SPIRE* wavelengths using the photometric and source density criteria. At the *PACS* wavelengths, the source density criterion leads to confusion limits 2 to 6 times higher than the photometric criterion with $q_{phot}=5$. For *SPIRE*, at $250 \mu\text{m}$, the limits obtained using the two criteria are very close and then, at longer wavelengths, the photometric quality constrains the confusion limit.

Extragalactic surveys will be conducted by both the *PACS* and *SPIRE* instruments. Up to now, the trade-off between large-area, shallow versus small-area, deep/ultra-deep observations has not been finalised. In the following two sections are examples of extragalactic surveys that could be done.

7.2.1 The *SPIRE* surveys

For large-area scan-mapping observations, the current estimates of time needed to map 1 square degree to an instrumental noise level of 3 mJy ($1\sigma_{inst}$) is about 1.7, 2 and 2.1 days at 250, 350 and $550 \mu\text{m}$ respectively (Matt Griffin, private communication). Three kinds of surveys could be done with *SPIRE* (Table 5):

(i) A very large-area (2 approximately $14^\circ \times 14^\circ$, i.e. ~ 400 square degrees) survey at the noise level of $5\sigma_{inst}=100$ mJy at $350\ \mu\text{m}$ (92 mJy at $250\ \mu\text{m}$ and 102 mJy at $550\ \mu\text{m}$).

(ii) A confusion-limited survey of about 100 square degrees. To reach a $5\sigma_{inst}$ noise limit of 14.1, 22.4 and 17.8 mJy, one needs 192, 90 and 149 days at 250, 350 and $550\ \mu\text{m}$ respectively.

(iii) A very deep survey, down to the confusion limit to extract as much information as possible about the underlying population. For example, mapping 8 square degrees to $5\sigma_{inst}=7.5$ mJy at $350\ \mu\text{m}$ would take 64 days.

We concentrate, in the following, on the $350\ \mu\text{m}$ band (although *SPIRE* is observing simultaneously the three bands). The number of detected sources for each survey is given in Table 5 and the redshift distribution in Fig. 14.

- The very large-area survey

This survey is well suited to the *Planck* sensitivity (Table 7). It would provide better positions for the *Planck* point sources and the combination with the *Planck* data would improve the spectral and spatial characterisation of foregrounds. It will take about 18 days, which is a small amount of time comparing to the enormous progress it would bring for the component separation problem for all observations in this wavelength range. The very-large-area survey will detect mostly nearby sources but hundreds of object could be detected at $z>1$. It will also explore the cirrus component. Moreover, thanks to its surface coverage, this survey will detect the rare and high- z objects for which little is known today.

- The confusion-limited survey:

For the confusion-limited survey, there are mainly two peaks in the redshift distribution: one at $z\sim 0$ due to the cold sources, the other between 0.8 and 3 being due to the starburst galaxies. The number of starburst galaxies detected between 0.8 and 3 doesn't vary much. Fig. 15 predicts the number of starburst galaxies that the confusion-limited survey will detect at $350\ \mu\text{m}$ per log-interval of luminosities (this figure does not include the cold population which contributes mostly locally). The evolution of the 10^{12} - $10^{13}\ L_\odot$ galaxies will be measured from $z\sim 0.5$ to 2.5. Galaxies with $L\sim 3\ 10^{11}\ L_\odot$ will be only accessible at $z\sim 0.1$. The nature and number of the highest luminosity objects are important to test cosmological theories, and thus populating the high redshift bins with enough objects to ensure $<14\%$ Poisson noise (corresponding to 50 sources) is a critical driver for the size of the sample, and accordingly, the area required for the survey. Based on our model, we see from Fig. 15 that to meet this $\sim 14\%$ goal for galaxies in the range $10^{12} - 10^{13}\ L_\odot$ at $z<2.5$, an area of 100 square degrees is the minimum required.

- The very-deep survey

The confusion-limited surveys will detect only $\sim 7\%$ of the CIB (1% for the very-large area survey). In this case, studying the fluctuations will bring informations on the underlying source population. The redshift distribution of sources making the bulk of the CIB and the fluctuations at $350\ \mu\text{m}$ are very similar. Thus, the fluctuations will be the unique opportunity to get information, particularly on sources that

dominate the CIB (sources with $L\sim 3\ 10^{11}\ L_\odot$), at redshifts where they cannot be detected individually. To detect and study them, a field with high signal-to-noise ratio is needed. Moreover, the size of the field should be large enough to try to detect the source clustering and not only be limited to the Poissonian noise detection (which is about $4300\ \text{Jy}^2/\text{sr}$). Since the source clustering is expected at the scales between 1 and 5 degrees (Knox et al. 2001), a field of about 8 square degrees is the minimum required. This field could be part of the confusion-limited survey which will be certainly split in several smaller area surveys.

7.2.2 The PACS surveys

For the whole field of view of $\sim 1.75' \times 3.5'$, the current estimates of time needed to reach $5\sigma_{inst}=3$ mJy is 1 hour (Albrecht Poglitsch, private communication). At 75, 110 and $170\ \mu\text{m}$, the confusion limits are about 0.13, 0.89, and 7.08 mJy, with $q_{density}$ of 8.9, 8.7 and 7.1 respectively. To reach the confusion limit for one field of view, i.e. $5\sigma_{inst}=0.1, 0.9$ and 7.1, we need 567, 11 and 0.18 hours at 75, 110 and $170\ \mu\text{m}$ respectively. Since for *PACS* the confusion limits and the time to reach those sensitivities are very different at the three wavelengths, three kinds of surveys could be done that, schematically, will probe the CIB in the three bands:

(i) A shallow survey of 20 square degrees down to the confusion limit at $170\ \mu\text{m}$. This survey is dedicated to probe the CIB at $170\ \mu\text{m}$ and study the correlations. Such a survey will take 88 days.

(ii) A deep survey down to the confusion limit at $110\ \mu\text{m}$. A good compromise between the covered surface and the time needed is a field of $25' \times 25'$ that will take about 67 days.

(iii) An ultra-deep survey down to the confusion limit at $75\ \mu\text{m}$ (or a little bit below the confusion limit). To map a $5' \times 5'$ field, 96 days are needed.

These three surveys correspond to about the same amount of time as the *SPIRE* surveys. Obviously, the *PACS* surveys have to be done within the same areas as the *SPIRE* ones.

PACS is observing simultaneously the 170 and $110\ \mu\text{m}$ channels or the 170 and $75\ \mu\text{m}$ channels. Ideally a combination $75/110\ \mu\text{m}$ and $75/170\ \mu\text{m}$ would have been preferable since the $170\ \mu\text{m}$ observation in the deep and ultra-deep surveys will not bring new science compared to the large area survey. On the contrary, observing the shortest wavelengths in the shallow survey will detect the very luminous, hot and rare galaxies that may be missed in the deep and ultra-deep surveys.

The three surveys will detect thousand of sources at $z\sim 1$ (Fig. 16) and will probe most of the CIB source population (they will resolve about 49, 77 and 87% of the CIB at 75, 110 and $170\ \mu\text{m}$ respectively, see Table 6).

At $170\ \mu\text{m}$, the shallow survey will give an unprecedented measurement of the evolution of the 10^{11} - $10^{12}\ L_\odot$ galaxies from $z\sim 0.25$ to 1 and the evolution of the 10^{12} - $10^{13}\ L_\odot$ galaxies from $z\sim 0.5$ to 3 (with enough objects to ensure $<10\%$ Poisson noise). Since half of the background is resolved into discrete sources at $170\ \mu\text{m}$, one complementary approach is to reduce the surface of the shallow survey to have a better

signal-to-noise ratio and thus study the underlying population. However, to study the correlation in the IR background, a minimum of 8 Sq. Deg. is required. A survey at $S_{min} = 8$ mJy, corresponding to $5\sigma_{inst}=3.7$ mJy, would take around 128 days for 8 Sq. Deg. Such a survey would give less statistics for the resolved sources but would help in understanding the whole CIB population. With a 8 Square Deg. field, the measure of the high luminosity source evolution would still be possible with a high degree of accuracy.

In conclusion, *PACS* will resolve about 80% of the CIB around 100 μ m (*SIRTF* will resolve at most around 55% of the CIB at 70 μ m and 20% at 160 μ m, Dole et al. 2002). It will definitely resolve the question of the population making the CIB near its emission's peak. It will measure with unprecedented accuracy the history of the IR-traced star formation up to $z \sim 1.5$. For the higher redshifts, the informations will come mainly from the *SPIRE* surveys. Although *SPIRE* will resolve less than 10% of the CIB in the submm, it will bring an unprecedented information on the evolution of galaxies up to $z \sim 3$ and also on the underlying population that will be very hard to detect from the ground due to the small area of the present surveys.

7.3 The Planck all-sky survey

For the *Planck* wavelengths, the confusion limits are given by the photometric criterion^{||}. With $q_{phot}=5$, they are about 447, 200, 79.4, 22.4 and 11.2 mJy at 350, 550, 850, 1380 and 2097 μ m respectively (for detection only, $q_{phot}=3$ is better and leads to the following confusion limits: 251, 112, 44.7, 14.1 and 6.31 at 350, 550, 850, 1380 and 2097 μ m respectively). The confusion limit (with $q_{phot}=5$) is above the 5σ instrumental noise at 350 μ m, comparable at 550 μ m and then below at longer wavelengths. It can be compared to the values given in the '*HFI proposal for the Planck mission (1998)*', Table 2.1. In this Table, the confusion limits have been computed using Ω rather than $\int f^2(\theta, \phi) d\theta d\phi$ in Eq. 12. This leads to a systematic overestimates of σ_{conf} by a factor 1.33. Correcting for this factor, the ratio of those estimates to the present ones increases from 350 to 2097 μ m from 1.2 to 3.

To compute the number of sources expected in the *Planck* survey, we use a cut in flux equal to $5\sigma_{tot}$ such as:

$$\sigma_{tot} = \sqrt{\sigma_{inst}^2 + \sigma_{conf}^2 + \sigma_{add}^2} \quad (15)$$

where σ_{conf} for *Planck* is given by $\sigma_{conf} = S_{lim}/5$. σ_{add} is an additional noise due to unresolved sources with fluxes between S_{lim} and $5\sigma_{inst}$:

$$\sigma_{add}^2 = \int f^2(\theta, \phi) d\theta d\phi \int_{S_{lim}}^{5\sigma_{inst}} S^2 \frac{dN}{dS} dS \quad (16)$$

This additional term is only present when the $5\sigma_{inst}$ is greater than the confusion limit (as for example for the *SPIRE* very-large survey).

^{||} The density criterion leads to $q_{density}$ from 1.5 to 0.8 from 350 to 2097 μ m respectively.

Final sensitivities on point sources, together with the number of detected sources for *Planck* are given in Table 7. At all wavelengths, the sensitivity of the survey is in the euclidian part of the number counts. *Planck* will not be able to constrain, with the resolved sources, the evolution of the submm galaxies but it will give an absolute calibration of the bright number counts, that will not be provided by any other planned instruments. Moreover, by covering the whole sky, it will probably detect the most spectacular dusty object of the observable Universe, as the hyperluminous or the strongly lensed starburst or AGN galaxies, as well as extreme sources not included in the model.

Note however that the sensitivities have been computed with an instrumental noise derived from a mean integration time. With the *Planck* scanning strategy, some high latitudes regions (where the cirrus contamination is low) will be surveyed more deeply, leading to an instrumental noise about 3 times lower. In such high redundancy parts of the sky, *Planck* survey will be limited by the confusion noise (except at 2097 μ m where the instrumental and confusion noises are on the same order). In those regions, *Planck* will produce unique maps of the CIB fluctuations. CIB anisotropies are mainly contributed by moderate to high redshift star-forming galaxies, whose clustering properties and evolutionary histories are currently unknown. *Planck* observations will thus complement the future far-IR and submm telescopes from ground and space that will perform deep surveys over small area. These surveys will resolve a substantial fraction of the CIB but will probably not investigate the clustering of the submm galaxies since it requires surveys over much larger areas.

7.4 Requirements for future experiments for very large deep surveys in the IR/submm/mm domain

Since the far-IR and submm sources (1) are often associated with mergers or interacting galaxies and (2) their energy output is dominated by high luminosity sources at high redshift (which might be related to the optical where the output is dominated by high brightness sources at high redshift (Lanzetta et al. 2002)), they have to be studied in detail in the long wavelength range and at high redshift ($z \geq 3$) as a tool to understand the merging process and the physics of the first non linear structures.

Two kinds of requirements have to be met by the post *SIRTF*, *Herschel* and *Planck* surveys:

- (i) They have to find the interesting high redshift sources which are early mergers made of building blocks not affected much yet by star formation and evolution. The number of such sources have to be large enough to do statistical studies.
- (ii) Once these sources are found, the future experiments have to have enough sensitivity and angular resolution to study them in details.

To quantify the first requirement, we compute the surface needed to detect more than 100 sources with luminosities of $3 \cdot 10^{11}$ and $3 \cdot 10^{12}$ L_{\odot} in each redshift range (Table 8). At high redshift, we need surveys of about hundred of square degrees to find enough high luminous objects to do

statistical studies. If enough area is covered, we need more-over a high sensitivity, for example we have to reach 0.21 mJy at 850 μm for $L=3 \times 10^{11} L_{\odot}$ galaxies (dominating the LF at $z \sim 1$) and 1.9 mJy at 850 μm (or 0.9 mJy at 1300 μm) for $L=3 \times 10^{12} L_{\odot}$ galaxies (dominating the LF at $z > 2$). The fluxes of typical $3 \times 10^{12} L_{\odot}$ galaxies at high- z are just, for the single-antenna telescopes, at the confusion limit. With the future wide-field imaging instruments on these telescopes, for example *SCUBA-2* (Holland et al. 2001) and *BOLO-CAM* (Glenn et al. 1998), hundred of square degrees at the 1 mJy level at 1300 μm could be mapped in a reasonable amount of time. However, with 10/15 arcsec beam, it will be very difficult to make optical identifications and follow-up observations at other wavelengths.

To reach the sensitivity of the $3 \times 10^{11} L_{\odot}$ galaxies at high- z , we need to have a very good angular resolution not to be limited by the confusion. Table 9 gives the angular resolution, together with the telescope diameter needed to reach 10, 30, 60 and 80 % of the CIB at 350, 850 and 1300 μm . To resolve 80% of the background at 1300 μm , we need a telescope diameter of about 173 m (!) and a diameter of about 113 m (!) at 850 μm and 23 m at 350 μm . In conclusion, finding the objects that are making the bulk of the CIB at long wavelengths will be a very challenging task! This leaves to an open question: how we find these objects? In the mid-IR, the Next Generation Space Telescope (NGST) will be a great tool. However, NGST observations will have two limitations: (1) the redshift up to which the dust component can be observed is limited to 4-5 and (2) the stellar component can be observed at higher z but the experience of combined optical/near-IR and far-IR observations shows how it is difficult to identify the galaxies which have most of their output energy in the Far-IR from optical and near-IR data alone. Therefore, the alternative today is to make the interferometres efficient enough to carry out large surveys.

For the second requirement, i.e study in detail the physics of the objects, observations have to have enough sensitivity to observe sub-components of the merging objects at high z (a $3 \times 10^{10} L_{\odot}$ sub-component at $z=5$ has a flux of about 0.014 mJy at 350 μm and of about 0.028 mJy at 850 μm). Moreover, an angular resolution of about 0.2 to 1 arcsec, together with spectroscopic capabilities are needed. For that, the submm and mm interferometres are the only tools, as shown by the recent spectacular observations of high-redshift quasar with the IRAM interferometre (Cox et al. 2002). Lower luminosity sources will require the *ALMA* (<http://www.eso.org/projects/alma/>, <http://www.mma.nrao.edu/>) or SPECS/SPIRIT (Leisawitz et al. 2001) interferometres.

7.5 The case of *ALMA*

Thanks to the negative K-correction, high redshift sources are accessible from the ground at submm and mm wavelengths. *ALMA*, a synthesis radio telescope (about 64 12-metre diameter telescopes) that will operate at submm and mm wavelengths will image the Universe with unprecedented sensitivity and angular resolution from the high-altitude Llano de Chajnantor, in northern Chile. It will be one of the largest ground-based astronomy project of the next decade after VLT/VLTI, and, together with the NGST,

one of the two major new facilities for world astronomy coming into operation by the end of the next decade. *ALMA*, with its angular resolution, great sensitivity and spectroscopic capabilities will reveal in detail, in the high- z galaxies, the astrophysical processes at work. Moreover, *ALMA* will be free of limitation due to source confusion and will therefore allow very faint galaxies to be detected. In this section, we discuss mostly *ALMA* abilities to find large enough samples of high redshift sources to do statistical studies and probe the CIB source population. Of course *ALMA* will be also used to study their structure and physics.

At 1300 μm , to find enough $\sim 3 \times 10^{11} L_{\odot}$ high- z sources, we need to cover a surface of at least 5 square degrees at a 5σ level of about 0.1 mJy (Table 8). Such a survey will resolve about 50% of the CIB. To resolve $\sim 80\%$ of the CIB, one needs to reach a 5σ level of about 0.02 mJy (Table 9). Therefore two kinds of surveys could be considered: a large-area (~ 5 Sq. deg.) and an ultra deep (~ 10 arcmin²) survey. For both surveys, the compact configuration has enough resolution not to be limited by the confusion. At 1300 μm , a 5σ detection of 2.3 mJy is reached in 1 sec for a beam area of 0.16 arcmin² (*ALMA* proposal for phase 2' and Blain 2001). This gives for the two types of surveys:

- The large-area survey: 5 Sq. Deg., $5\sigma_{1300} = 0.1$ mJy (50% of the CIB)
A 1 square degree field requires 22 500 pointings, each with 529 seconds of observations, for a total of 138 days. For 5 Sq. Deg., 690 days are needed, i.e. 1.9 years.
- The ultra-deep survey: 10 arcmin², $5\sigma_{1300} = 0.02$ mJy (80% of the CIB)
A 10 arcmin² field requires 625 pointings, each with 13225 seconds of integration, for a total of 96 days.

In conclusion, if we want to achieve the two goals: (i) detect enough early mergers made of building blocks not affected much yet by star formation and evolution and (ii) probe most of the CIB source population at large wavelengths, we will have to do extragalactic surveys with *ALMA* using a substantial fraction of the time to find the sources. Such large surveys including the whole *ALMA* collaboration would be much more efficient in terms of scientific progress than smaller area surveys conducted by individual smaller teams.

8 SUMMARY

We have developed a phenomenological model that constrains in a simple way the IR luminosity function evolution with the redshift, and fits all the existing source counts and redshift distribution, CIB intensity and for the first time CIB fluctuations observations from the mid-IR to the submm range. The model has been used to give some predictions for future *Herschel* deep survey observations and the all-sky *Planck* survey. It comes out that the planned experiments (*SIRTF*, *Herschel*, *Planck*) will be mostly limited by the confusion. To find out a large number of objects that dominate the LF at high redshift ($z > 2$), future experiments need both the angular resolution and sensitivity. This can be achieved in the submm only thanks to interferometres

such as *ALMA*. However, mapping large fractions of the sky with high signal-to-noise ratio will take a lot of time (for example, 1.9 years to map 5 square degrees that resolve 50% of the CIB at 1.3 mm with *ALMA*).

APPENDIX A:

We provide, in an electronic form through a web page^{**}, a distribution of the model's outputs and programs (to be used in IDL) containing:

- The array $dN/(d\ln L dz)$ as a function of L and z , dS/dz as a function of L and z and S_ν in Jy for each luminosity and redshift, from 10 to 2000 μm and the evolution of the LF for both the normal and the starburst populations (for $\Omega_\Lambda=0.7$, $\Omega_0=0.3$ and $h=0.65$)
- Some usefull programs that compute the integral counts, detected sources, CIB and fluctuations redshift distribution, and the level of the fluctuations from the previous data cubes.

Acknowledgements: HD thanks the *MIPS* project (under NASA Jet Propulsion Laboratory subcontract # P435236) for support during part of this work and the Programme National de Cosmologie and the Institut d'Astrophysique Spatiale for some travel funding.

REFERENCES

- Almaini O., Lawrence A., Boyle B.J., 1999, MNRAS 305, 59
 Altieri B., Metcalfe L., Kneib J.P. et al., 1999, A&A 343L, 65
 Aussel H., Cesarsky C.J., Elbaz D., Stark J.L., 1999, A&A 342, 313
 Balland C., Devriendt J.E.G., Silk J., 2002, MNRAS, to be submitted
 Barger A.J., Cowie L.L., Mushotzky R.F., Richards E.A., 2001, AJ 121, 662
 Barger A.J., Cowie L.L., Sanders D.B., 1999, ApJ 518, L5
 Bertin E., Dennefeld M., Moshir M., 1997, A&A 323, 685
 Bertoldi F., Menten K.M., Kreysa E., Carilli C.L., Owen F., 2001, in Proc JD9, IAU Manchester 2001, "Cold gas and Dust at High Redshift", D.J. Wilner Ed., Highlights of Astronomy Vol. 12 PASP, in press (astro-ph/0010553)
 Bertoldi F. et al., 2000, in "Cold Gas and Dust at High Redshift", 24th meeting of the IAU, Joint Discussion 9
 Biller S.D., Buckley J., Burdett A., et al., 1998, Phys. Rev. Lett. 80, 2992
 Biviano A., Metcalfe L., Altieri B., ASP volume proceedings of the 1999 Marseille IGRAP conference 'Clustering at High Redshifts', A. Mazure, O. Le Fevre, V. Le Brun Eds (astro-ph/9910314)
 Blain A.W., 2001, in 'Science with the Atacama Large Millimeter Array', A. Wootten ed. ASP Conf. Ser. Vol. 235 (ASP: San Francisco) pp. 261-270 (astro-ph/9911449)
 Blain A.W., Kneib J.-P., Ivison R.J. et al., 1999, ApJ 512, L87
 Borys C., Chapman S., Halpern M. et al., 2002, MNRAS, in press
 Carilli C.L., Bertoldi F., Bertarini A. et al., 2000, in 'Deep Millimeter Surveys: Implications for Galaxy Formation and Evolution,' eds. Lowenthal and Hughes, World Scientific (astro-ph/0009298)
 Cesarsky C.J., Abergel A., Agnese P. et al., 1996, A&A 315, 32
 Chapman S.C., Scott D., Steidel C. et al., 2000, MNRAS 319, 318
 Chapman S.C., Scott D., Steidel C. et al., 2002a, to be submitted
 Chapman S.C., Scott D., Steidel C. et al., 2002b, ApJ 573, 66
 Charry R. & Elbaz D., 2001, ApJ 556, 562
 Clements C., Désert F.X., Franceschini A., et al., 1999, A&A 346, 383
 Cohen J., Hogg D.W., Blandford R. et al., 2000, ApJ 538, 29
 Cox P., Omont A., Djorgovski S.G. et al., 2002, A&A 387, 406
 Dale D., Helou G., Contursi A. et al., 2001, ApJ 549, 215
 de Bernardis P., P.A.R. Ade, J.J. Bock et al., 2002, ApJ 564, 559
 Désert F.X., Boulanger F., Puget J.-L., 1990, A&A 327, 215
 Devriendt J.E.G., Guiderdoni B., 2000, A&A 363, 851
 Dwek E., Arendt R.G., Hauser M.G. et al., ApJ 508, 106
 Dole H., Lagache G., Puget J.-L., 2002, ApJ, submitted
 Dole H., Gispert R., Lagache G. et al., 2001, A&A 372, 364
 Dole H., Gispert R., Lagache G. et al., 2000, in "ISO Surveys of a Dusty Universe", Springer 'Lecture Notes in Physics', D. Lemke, Stickel, Wilke K. Eds., p 54 (astro-ph/0002283)
 Dunne L. & Eales S.A., 2001, MNRAS 327, 697
 Dunne L., Eales S.A., Michael E. et al. 2000, MNRAS 315, 115
 Dwek E., Arendt R.G., Hauser M.G., et al., 1998, ApJ 508, 106
 Eales S., Lilly S., Webb T. et al., 2000, AJ 120, 2244
 Eales S., Lilly S., Walter G. et al., 1999, ApJ 515, 518
 Elbaz D., Cesarsky C.J., Chanial P. et al., 2002, A&A 384, 848
 Elbaz D., Cesarsky C.J., Fadda D. et al., 1999, A&A 351, 37
 Ellis R.S., 1997, ARA&A 35, 389
 Fabian A.C., Smail I., Iwasawa K. et al., 2000, MNRAS 315, 8
 Fadda D., Flores H., Hasinger G. et al., 2002, A&A 383, 838
 Finkbeiner D.P., Davis M., Schlegel D.J., 2000, ApJ 544, 81
 Flores H., Hammer F., Désert F.-X. et al. 1999a, A&A 343, 389
 Flores H., Hammer F., Thuan T.X. et al. 1999b, ApJ 517, 148
 Fixsen D.J., Dwek E., Mather J.C. et al. 1998, ApJ 508, 123
 Ford H.C., Tsvetanov Z.I., Ferrarese L., Jaffe, W., 1998, in IAU Symp. 184, The Central Regions of the Galaxy and Galaxies, ed. Y Sofue (Kluwer: Dordrecht)
 Franceschini A., Aussel H., Cesarsky C.J. et al. 2001, A&A 378, 1
 Franceschini A., Andreani P., Danese L., 1998, MNRAS 296, 709
 Freedman W.L., Madore B.F., Gibson B.K. et al., 2001, ApJ 553, 47
 Gispert R., Lagache G., Puget J.-L., 2000, A&A 360, 1
 Glenn J., Bock J.J., Chattopadhyay G. et al., 1998, SPIE, Vol. 3357, p. 326
 Guiderdoni B., 2001, Abstracts from SF2A-2001: Semaine de l'Astrophysique Française, Eds.: Societe Française d'Astronomie et d'Astrophysique, published by EdP-Sciences, Conference Series, p.68
 Guiderdoni B., Hivon E., Bouchet F., Maffei B., 1998, MNRAS 295, 877
 Gregorich D.T., Neugebauer G., Soifer B.T., Gunn J.E., Herter T.L., 1995, AJ 110, 259
 Hacking P.B., Houck J.R., 1987, ApJS 63, 311
 Hatton S., Devriendt J.E.G., Ninin S. et al., 2002, submitted to MNRAS
 Hauser M.G., Dwek E., 2001, ARAA, 37, 249
 Hauser M.G., Arendt R.G., Kelsall T. et al., 1998, ApJ 508, 25
 Hughes D.H., Dunlop J.S., Rowan-Robinson M. et al., 1998, Nature 394, 241
 Holland W.S., Duncan W.D., Audley M.D. et al., 2001, AAS Meeting 199, #103.06
 Holland W. S., Cunningham C.R., Gear, W.K. et al., 1998, SPIE Vol. 3357, p. 305-318, Advanced Technology MMW, Radio, and Terahertz Telescopes, Thomas G. Phillips Ed.
 Hornschemeier A.E., Brandt W.N., Garmire G.P. et al., 2000, ApJ 541, 49
 Helou, G., 2000., in "Infrared space astronomy, today and tomorrow", Les Houches, Session LXX. Edited by F. Casoli, J.

^{**} http://www.ias.fr/PPERSO/glagache/act/gal_model.html

- Lequeux, and F. David. Published in cooperation with the NATO Scientific Affair, Springer-Verlag, p.337
- Juvela M., Mattila K., Lemke D., 2000, *A&A* 360, 813
- Kakazu Y., Sanders D.B., Joseph R.D. et al., 2002, *astro-ph/0201326*
- Kawara K., Sato Y., Matsuhara H. et al. 1998, *A&A* 336, L9
- Kessler M.F., Steinz J.A., Anderegg M.E. et al. 1996, *A&A* 315, 27
- Kim D.-C., Sanders D.B., 1998, *ApJSS* 119, 41
- Kiss Cs., Ábrahám P., Klaas U. et al., 2001, *A&A* 379, 1161
- Knox L., Cooray A., Eisenstein D., Haiman Z., 2001, *ApJ* 550, 7
- Klaas U., Haas M. Muller S.A.H. et al., 2001, *A&A* 379, 823
- Lagache G., Puget J.-L., 2000 *A&A* 355, 17
- Lagache G., Haffner L.M., Reynolds R.J., Tufte S.L., 2000, *A&A* 354, 247
- Lagache, G., Abergel, A., Boulanger F. et al., 1999, *A&A* 344, 322
- Lanzetta K.M., Yahata N., Pascarelle S. et al., 2002, *ApJ* 570, 492
- Leisawitz D., et al., 2001, in “Tetons 4: Galactic Structure, Stars and the Interstellar Medium”, ASP Conference Series, Vol. 231. Edited by Charles E. Woodward, Michael D. Bica, and J. Michael Shull. San Francisco: Astronomical Society of the Pacific. ISBN: 1-58381-064-1, p.639
- Lemke D., Klaas U., Abolins J. et al., 1996, *A&A* 315, 64
- Lilly S.J., Eales S.A., Gear W.K.P. et al., 1999, *ApJ* 518, 641
- Linden-Vornle M.J.D., Norgaard-Nielsen H.U., Jorgensen H.E. et al. 2000, *A&A*, 353, L51
- Lonsdale C.J., Hacking P.B., Conrow T.B., Rowan-Robinson M., 1990, *ApJ* 358, 20
- Lutz D., Genzel R., Kunze D. et al., 1999, *Ap&SS* 266, 85
- Maffei 1994, PhD Thesis, Université de Paris XI
- Malkan M.A., Stecker F.W., 2001, *ApJ* 555, 641
- Matsuhara H., Kawara K., Sato Y. et al. 2000, *A&A* 361, 407
- Metcalfe L., 2000, in “The Extragalactic Infrared Background and its cosmological implications”, IAU Symposium 204, p. 18
- Miville-Deschênes M.-A., Lagache G., Puget J.-L., 2002, *A&A*, in press
- Page M.J., Stevens J.A., Mittaz J.P.D. and Carrera F.J., 2002, *Science*, 294, 2516 (*astro-ph/0202102*)
- Patris J., Dennefeld M., Lagache G., Dole H., 2002, submitted to *A&A*
- Pearson C.P., 2001, *MNRAS* 325, 1511
- Perrotta F., Magliocchetti M., Baccigalupi C. et al., submitted to *MNRAS* (*astro-ph/0111239*)
- Perlmutter S., Aldering G., Goldhaber G. et al., 1999, *ApJ* 517, 565
- Pilbratt G.L., 2001, in Proc. of ‘The Promise of the Herschel Space Observatory’ symposium held 12-15 December 2000 in Toledo, Spain, eds. G.L.Pilbratt, J.Cernicharo, A.M.Heras, T.Prusti, R.Harris, ESA SP-460, pp. 13-20
- Poggianti B.M., Wu H., 2000, *ApJ* 529, 157
- Poggianti B.M., Bressan A., Franceschini A., 2001, *ApJ* 550, 195
- Poggianti B.M., Smail I., Dressler A. et al., 1999, *ApJ* 518, 576
- Puget J.-L., Abergel A., Bernard J.-P. et al., 1996, *A&A* 308, L5
- Puget J.L., Lagache G., Clements D.L. et al., 1999, *A&A* 354, 29
- Rigopoulou D., Franceschini A., Aussel H. et al., 2000, *ApJ* 537, 85
- Renault C., Barrau A., Lagache G., Puget J.-L., 2001, *A&A* 371, 771
- Rowan-Robinson M., 2001, *ApJ* 549, 745
- Rowan-Robinson M., Hughes J., Veda K., Walker D.W., 1990, *MNRAS* 289, 490
- Sajina A., Borys C., Chapman S. et al., 2002, to be submitted
- Sanders D.B., Mirabel I.F., 1996, *ARA&A* 34, 749
- Saunders W., Rowan-Robinson M., Lawrence A. et al. 1990, *MNRAS* 242, 318
- Schlegel D.J., Finkbeiner D.P., Davis M. 1998, *ApJ* 500, 525
- Scott S.E., Fox M.J., Dunlop J.S. et al., 2002, *MNRAS* 331, 817
- Serjeant S., Efstathiou A., Oliver S. et al., 2001, *MNRAS* 322, 262
- Serra G., Puget J.-L., Ryter C.E., Wijnbergen J.J., 1978, *ApJ* 222, 21
- Severgnini P., Maiolino R., Salvati, M. et al., 2000, *A&A* 360, 457
- Silverberg R.F., Hauser M.G., Mather J.C. et al. 1979, *SPIE* 172, 149
- Smail I., Ivison R.J., Blain, A.W., Kneib J.-P. et al., 1998, *ApJ* 507, 21
- Smail I., Ivison R.J., Blain A.W., 1997, *ApJ* 490, L5
- Soifer B.T., Neugebauer G., 1991, *AJ* 101, 354
- Stickel M., Lemke D., Klaas U. et al., 2000, *A&A* 359, 865
- Stickel M., Bogun S., Lemke D. et al., 1998, *A&A* 336, 116
- Takeuchi T.T., Ishii T.T., Hirashita H. et al., 2001, *PASJ* 53, 37
- Trentham N., Kormendy J., Sanders D.B., 1999, *AJ* 117, 2152
- Veilleux S., Kim D.-C., Sanders D.B., 1999, *ApJ* 522, 113
- Wang Y.P., 2002, *A&A* 383, 755
- Wang Y.P., Biermann P.L., 2000, *A&A* 356, 808
- Webb T.M.A., Eales S.A., Lilly S.J. et al., 2002, submitted to *ApJ*
- Xu C., Lonsdale C.J., Shupe D.L. et al. 2001, 562, 179

This paper has been produced using the Royal Astronomical Society/Blackwell Science \LaTeX style file.

Table 2. Predicted CIB intensity at 15 μm (*ISOCAM* filter), 60 and 100 μm (IRAS filters), 170 μm (*ISOPHOT* filter), 350 μm (filter such as $\Delta\lambda / \lambda = 1/3$) and 850 μm (*SCUBA* filter) compared to measurements.

λ μm	Predicted CIB MJy/sr	Predicted CIB $\text{Wm}^{-2}\text{sr}^{-1}$	Measured CIB $\text{Wm}^{-2}\text{sr}^{-1}$	
15	$1.25 \cdot 10^{-2}$	$2.5 \cdot 10^{-9}$	$> 2.4 \pm 0.5 \cdot 10^{-9}$	(1)
60	0.12	$6.1 \cdot 10^{-9}$	-	
100	0.35	$1.1 \cdot 10^{-8}$	$\sim 1.5 \cdot 10^{-8}$	(2)
170	0.76	$1.3 \cdot 10^{-8}$	$1.4 \pm 0.3 \cdot 10^{-8}$	(3)
350	0.76	$6.5 \cdot 10^{-9}$	$5.63^{+4.30}_{-2.80} \cdot 10^{-9}$	(4)
850	0.20	$6.9 \cdot 10^{-10}$	$5.04^{+4.31}_{-2.61} \cdot 10^{-10}$	(4)

(1) Elbaz et al. (2002)

(2) Renault et al. (2001)

(3) From Kiss et al. (2001) and extrapolation of DIRBE measurements

(4) From Fixsen et al. (1998) and Lagache et al. (1999)

Table 3. Comparison of the predicted CIB fluctuations (for $S < S_{max}$ in Jy^2/sr) and the observations.

λ (μm)	S_{max} (mJy)	Observations (Jy^2/sr)	References	Model (Jy^2/sr)
170	1000	~ 25000	Sorel et al., in prep	23694
170	250	13000 ± 3000	Matsuhara et al. 2000	15644
170	100	7400	Lagache & Puget 2000	11629
100	700*	5800 ± 1000	Miville-Deschênes et al. 2002	10307
90	150	12000 ± 2000	Matsuhara et al. 2000	5290
60	1000	1600 ± 300	Miville-Deschênes et al. 2002	2507

* Bright sources in Miville-Deschênes et al. (2002) are removed at 60 and 100 μm using the cut of 1 Jy at 60 μm . Since the 60 μm sources are mostly starburst galaxies, we estimate that 1 Jy at 60 μm is equivalent to 0.7 Jy at 100 μm .

Table 4. *PACS* and *SPIRE* 1σ confusion noise and its associated flux limit (S_{lim}) for the photometric criterion ($q_{phot}=5$) and the source density criterion (with the equivalent $q_{density}$).

		σ (mJy)	S_{lim} (mJy)
<i>PACS</i> 75 μm	$q_{phot}=5.0$	$2.26 \cdot 10^{-3}$	$1.12 \cdot 10^{-2}$
	$q_{density}= 8.9$	$1.42 \cdot 10^{-2}$	$1.26 \cdot 10^{-1}$
<i>PACS</i> 110 μm	$q_{phot}=5.0$	$1.98 \cdot 10^{-2}$	$1.0 \cdot 10^{-1}$
	$q_{density}= 8.7$	$1.02 \cdot 10^{-1}$	$8.91 \cdot 10^{-1}$
<i>PACS</i> 170 μm	$q_{phot}=5.0$	$3.97 \cdot 10^{-1}$	2.00
	$q_{density}= 7.13$	$9.93 \cdot 10^{-1}$	7.08
<i>SPIRE</i> 250 μm	$q_{phot}=5.0$	2.51	12.6
	$q_{density}=5.2$	2.70	14.1
<i>SPIRE</i> 350 μm	$q_{phot}=5.0$	4.4	22.4
	$q_{density}= 3.6$	3.52	12.6
<i>SPIRE</i> 550 μm	$q_{phot}=5.0$	3.69	17.8
	$q_{density}=2.5$	3.18	7.94

Table 5. Designed surveys that could be done with *SPIRE* (Numbers are from the 350 μm channel).

Surface (Sq. Deg.)	$5\sigma_{inst}$ (mJy)	$5\sigma_{conf}$ (mJy)	$5\sigma_{tot}$ (mJy)	Days	Number of sources	% resolved CIB
400	100	28.2 ¹	103.9	18	4768	1
100	15.3	22.4	27.1	192	33451	6.7
8	7.5	22.4	23.6	64	3533	7.8

¹ Unresolved sources below $5\sigma_{inst} = 100$ mJy induce a confusion noise of $\sigma_{conf} = 5.63$ mJy.

Table 6. Designed surveys that could be done with *PACS*.

Surface	λ (μm)	Days ^a	$5\sigma_{inst}$ (mJy)	S_{min} ^b (mJy)	Number of sources	% resolved CIB
20 Sq. Deg.	170	88	7.08	10.01	87 322	48.7
625 Sq. Arcmin	110	67	0.89	1.26	1955	77
25 Sq. Arcmin	75	96	0.13	0.18	192	87

^a Depending on the scanning/chopping/beam switching strategy, there may be some overhead of about 20%

$$^b S_{min} = \sqrt{(5\sigma_{inst})^2 + S_{lim}^2} = \sqrt{2} \times S_{lim}$$

Table 7. *Planck* sensitivities ($5\sigma_{inst}$), confusion limit ($S_{lim} = 5\sigma_{conf}$), confusion induced by sources between S_{lim} and $5\sigma_{inst}$ ($5\sigma_{add}$), and total 5σ noise (which is the quadratic sum of the contribution from the detector noise and the extragalactic confusion noise). Also given are the cold, starburst and total galaxy densities.

λ (μm)	$5\sigma_{inst}$ (mJy)	$5\sigma_{conf}$ (mJy)	$5\sigma_{add}$ (mJy)	$5\sigma_{tot}$ (mJy)	$N_{cold}(S > 5\sigma_{tot})$ (/sr)	$N_{SB}(S > 5\sigma_{tot})$ (/sr)	$N(S > 5\sigma_{tot})$ (/sr)
350	216.5	447	0	497	1342	40	1382
550	219	200	7.9	297	187	15	202
850	97	79.4	3.2	125	72	8	80
1380	57.5	22.4	2.6	62	35	4	39
2097	41.5	11.2	2.4	43	23	3	26

Table 8. Sky area in square degrees to be covered to detect more than 100 sources in a redshift range $\Delta z/z=0.3$, for $3 \times 10^{11} L_{\odot}$ (top) and $3 \times 10^{12} L_{\odot}$ (bottom) starburst galaxies.

$3 \times 10^{11} L_{\odot}$	z	S ₃₅₀ (mJy)	S ₈₅₀ (mJy)	S ₁₃₀₀ (mJy)	Surface
	1	2.95	0.30	0.09	0.7
	3	0.78	0.25	0.08	1.8
	5	0.21	0.26	0.11	10
	7	0.065	0.21	0.12	60
$3 \times 10^{12} L_{\odot}$	z	S ₃₅₀ (mJy)	S ₈₅₀ (mJy)	S ₁₃₀₀ (mJy)	Surface
	1	22.1	2.05	0.7	5.7
	3	7.51	1.82	0.6	6.1
	5	2.73	2.07	0.8	53
	7	1.01	1.89	0.9	398

Table 9. Angular resolution and telescope diameter needed to have the confusion limit at a flux level S_{min} such that sources above S_{min} contribute for about 10, 30, 60 and 80 % of the CIB (top: 350 μm , middle: 850 μm , bottom: 1300 μm).

% CIB	S ₃₅₀ (mJy)	Log N (/sr)	θ^a (arcsec)	D ^b (metres)
80	0.9	8.01	3.2	23
60	2.5	7.71	4.8	15.1
30	8	7.09	10	7.2
10	18	6.32	23.7	3.0
% CIB	S ₈₅₀ (mJy)	Log N (/sr)	θ^a (arcsec)	D ^b (metres)
80	0.05	8.35	1.6	113
60	0.2	8.03	3.0	59
30	1	7.45	7.0	25
10	2	6.77	15.3	12
% CIB	S ₁₃₀₀ (mJy)	Log N (/sr)	θ^a (arcsec)	D ^b (metres)
80	0.02	8.38	1.6	173
60	0.06	8.10	2.7	101
30	0.3	7.48	6.6	40
10	0.7	6.75	15.6	17

^a θ has been computed using $N \times \theta^2 = 1/30$ ^b $D = \lambda / \theta$

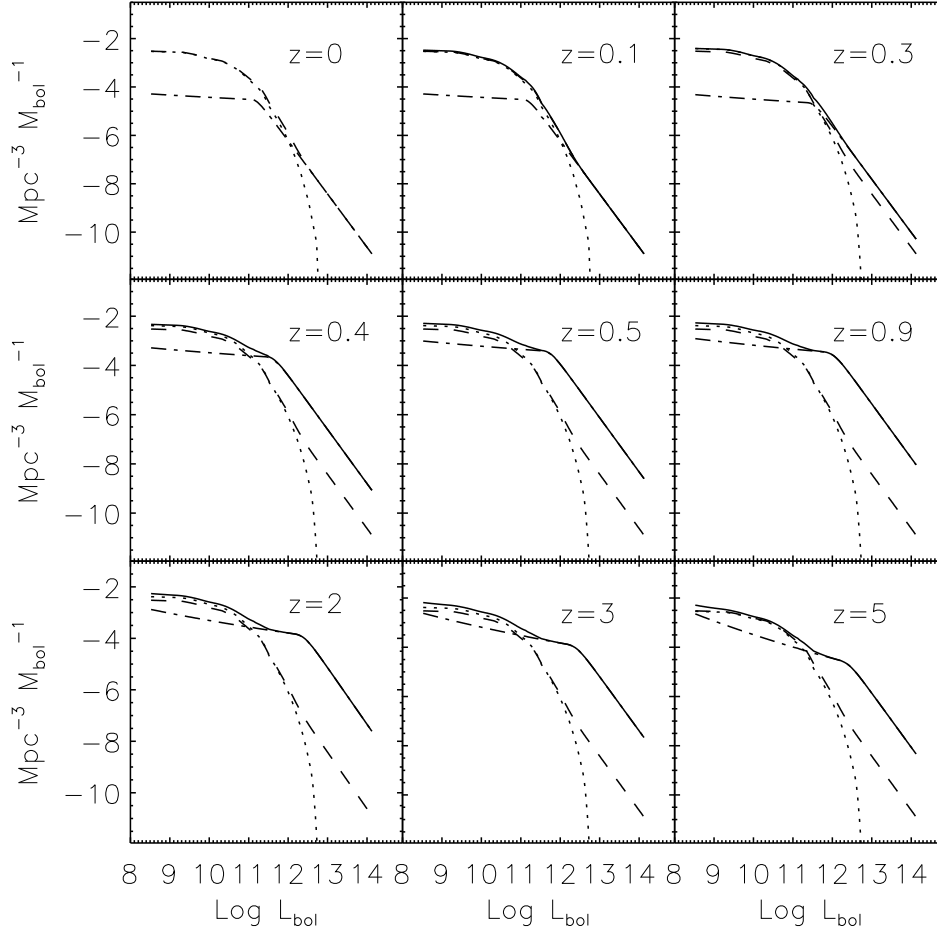


Figure 7. Co-moving evolution of the luminosity function. The dotted line is for the normal galaxies and the dotted-dashed line, for the starburst galaxies. The continuous lines corresponds to both starburst and normal galaxies and the dashed line is the LF at $z=0$ for comparison.

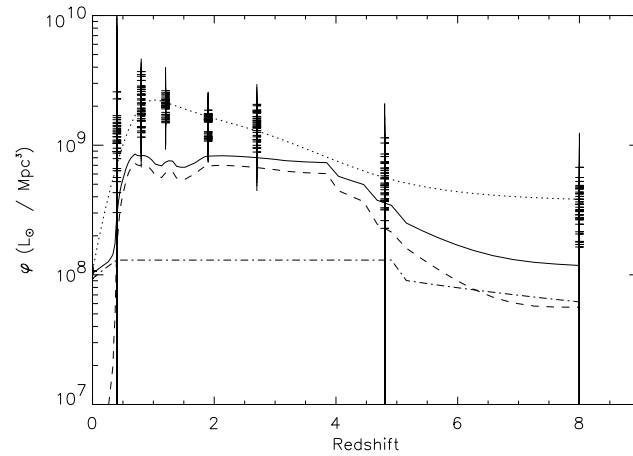


Figure 8. Co-moving luminosity density distribution for the starburst galaxies (dash line), normal galaxies (dot-dash line), and both normal and starburst galaxies (continuous line). Also shown for comparison is the co-moving luminosity density distribution from all cases of Gispert et al. 2001 (crosses with error bars), together with the best fit passing through all cases (dot line).

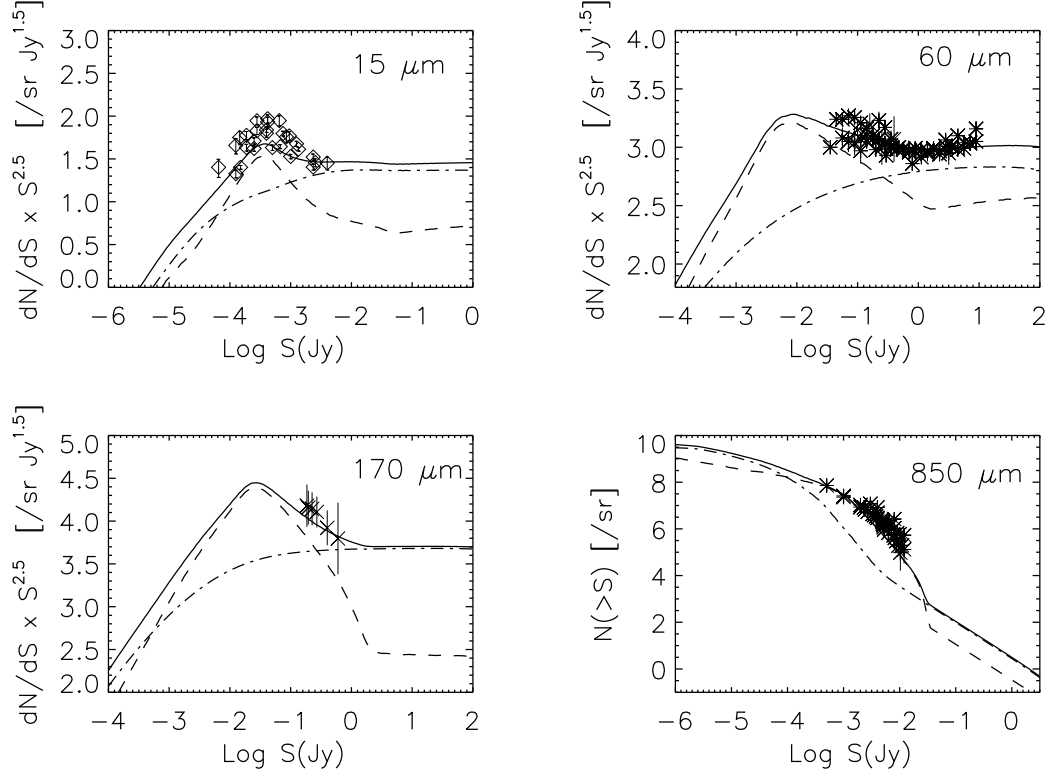


Figure 9. Number counts at 15, 60, 170 and 850 μm (in Log) together with the model predictions (starburst galaxies: dash line, normal galaxies: dot-dash line, both normal and starburst galaxies: continuous line). Data at 15 μm are from Elbaz et al. (1999), at 170 μm from Dole et al. (2001), at 60 μm from Hacking & Houck (1987), Gregorich et al. (1995), Bertin et al. (1997), Lonsdale et al. (1990), Saunders et al. (1990) and Rowan-Robinson et al. (1990) and at 850 μm from Smail et al. (1997), Hughes et al. (1998), Barger et al. (1999), Blain et al. (1999), Borys et al. (2001), Scott et al. (2002) and Webb et al. (2002).

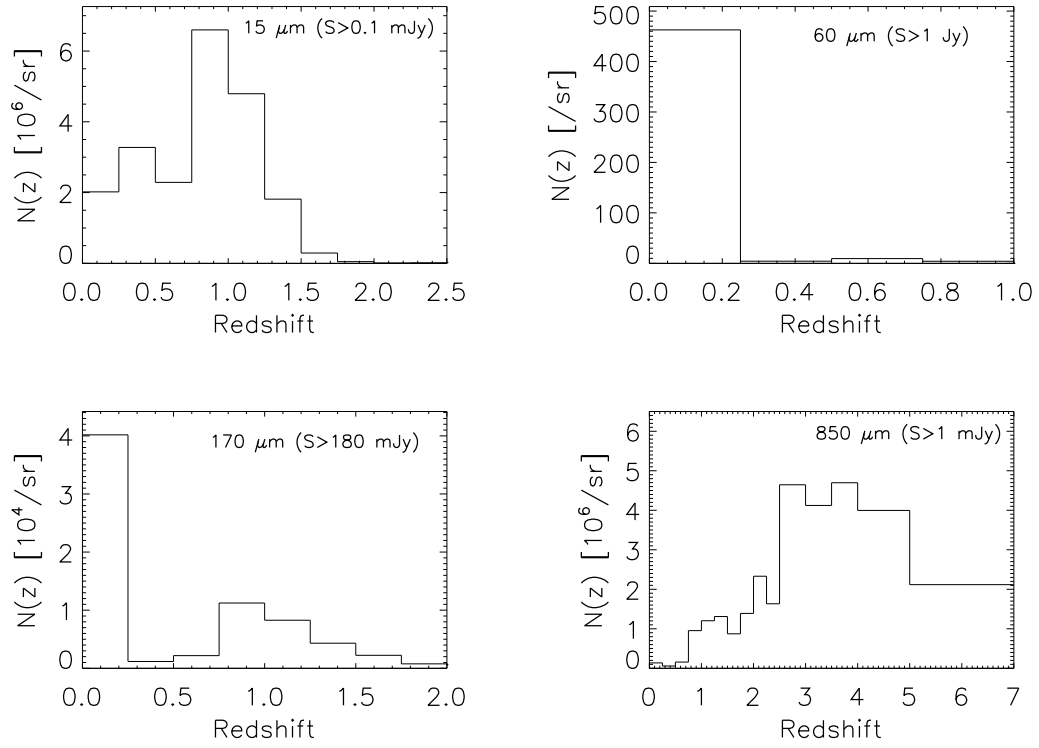


Figure 10. Predicted redshift distribution for resolved sources at 15, 60, 170 and 850 μm .

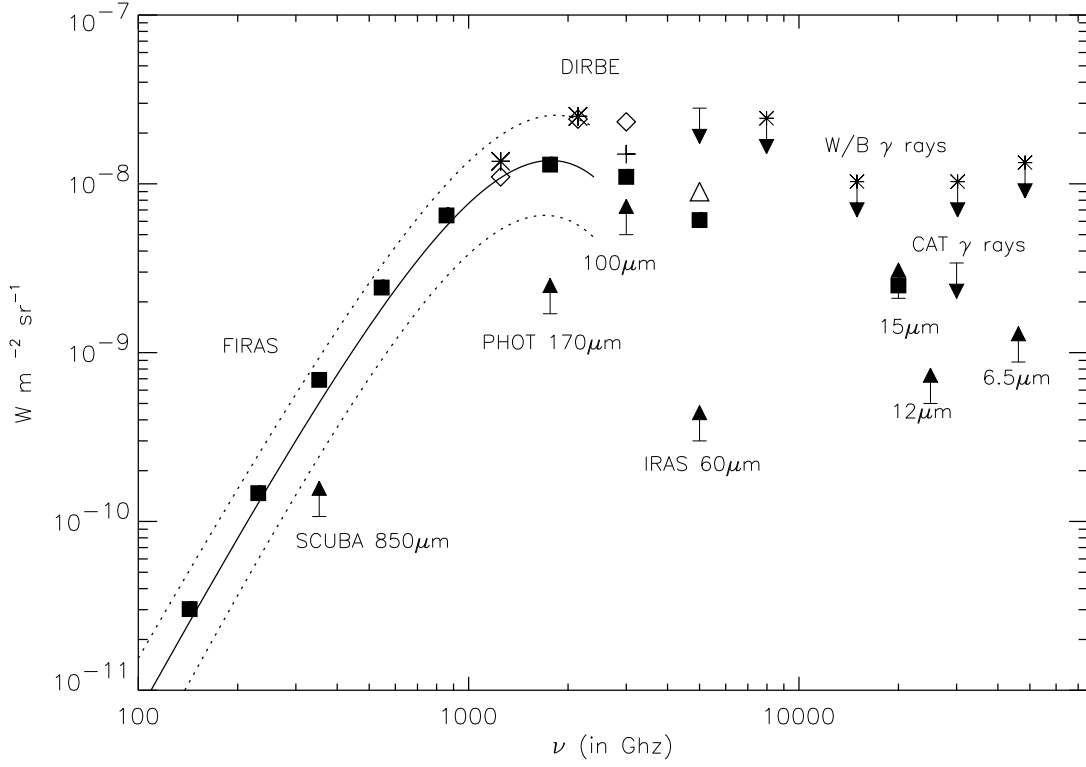


Figure 11. Cosmic Background from mid-IR to the millimetre wavelength. The 6.5 (Désert, private communication), 12 (Clements et al. 1999) and 15 μm (Elbaz et al 2002) lower limits come from ISOCAM number counts; the upper limit “CAT” is from Renault et al. (2001) and the cross upper limits W/B are from Biller et al. (1998). At longer wavelength, we have the 60 μm estimate from Miville-Deschênes et al. 2002 (Δ), the upper limit from Finkbeiner et al. (2000), and the lower limit from number counts at 60 μm (Lonsdale et al. 1990); at 140 and 240 μm are displayed the Lagache et al. 2000 (\diamond) and Hauser et al. 1998 (\star) DIRBE values; at 100 μm is given the lower limit from Dwek et al. (1998) together with the estimates from Renault et al. 2001 (+) and the determination of Lagache et al. 2000 (\diamond); at 170 (Puget et al. 1999) and 850 μm (Barger et al. 1999) are lower limits from number counts. The analytic form of the CIB at the FIRAS wavelengths is from Fixsen et al. (1998). The CIB derived from the model at selected wavelengths is given by filled squares.

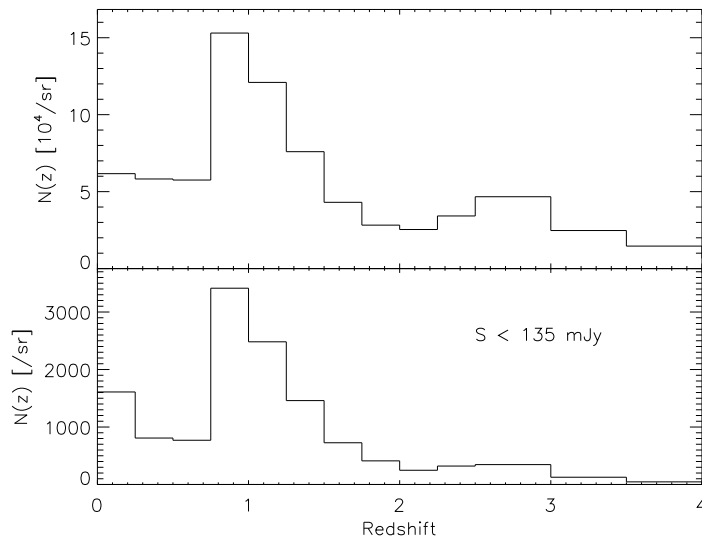


Figure 12. Redshift distribution of sources making the CIB intensity and its fluctuations ($S < 135$ mJy) at 170 μm .

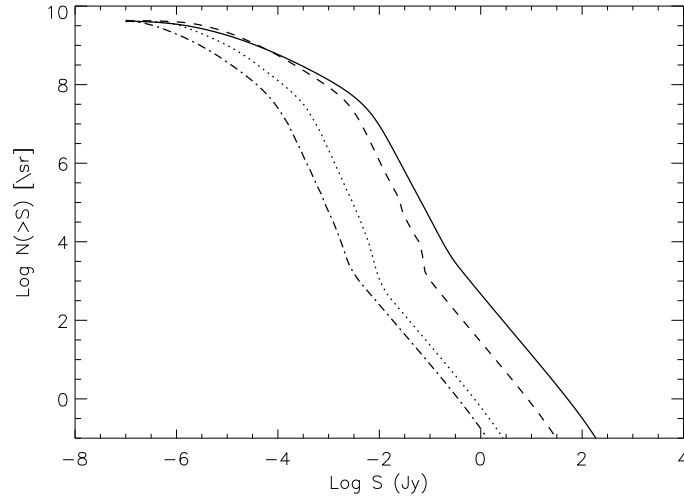


Figure 13. Predicted Number counts at 350 (continuous line), 550 μm (dashed line), 1300 μm (dotted line) and 2097 μm (dotted-dashed line).

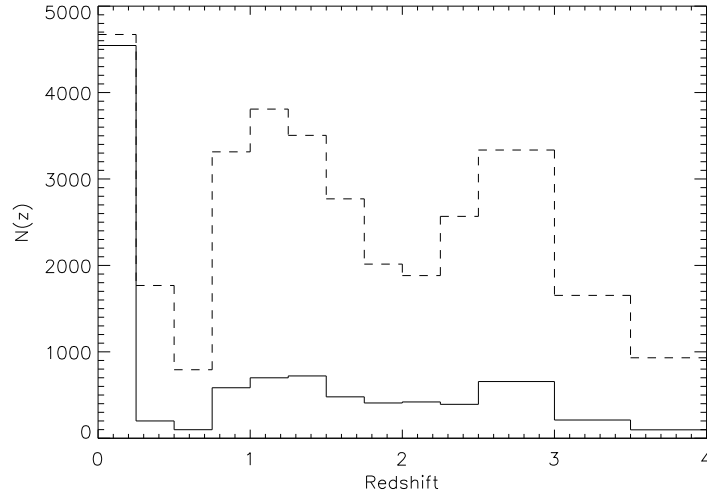


Figure 14. *SPIRE* 350 μm redshift distribution for sources detected in the very-large area survey (continuous line, $S > 103.9$ mJy, multiplied by 2) and the confusion-limited survey (dashed line, $S > 27.1$ mJy).

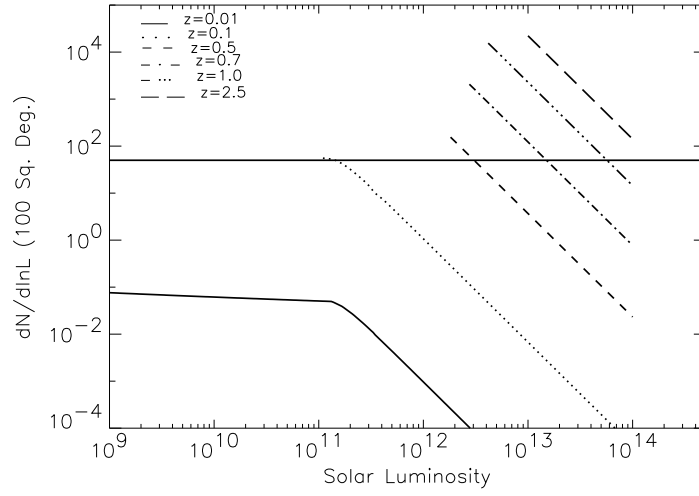


Figure 15. Number of starburst galaxies that can be detected in different redshift ranges (with a $\Delta z/z=0.5$) at $350\ \mu\text{m}$ by the confusion limited survey of 100 square degrees as a function of bolometric luminosity. The horizontal line shows the 50 sources needed in a $\Delta z/z=0.5$ bin for $\sim 14\%$ accuracy. The plots are limited to the fluxes above the detection limit and to luminosities below $10^{14}\ L_{\odot}$.

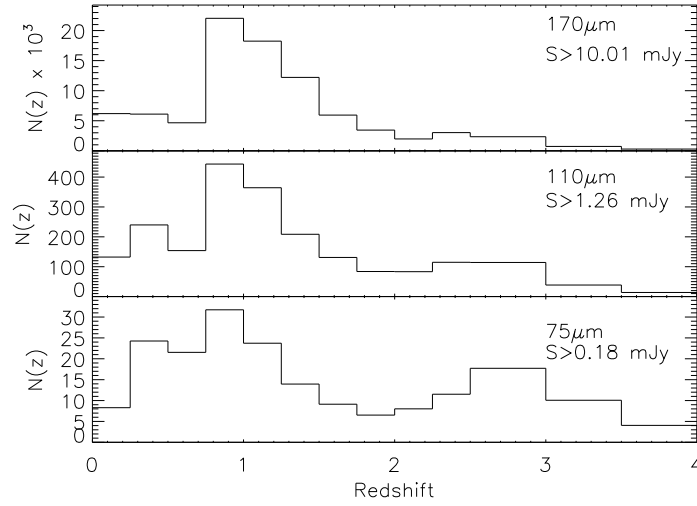


Figure 16. From bottom to top: redshift distribution for the ultra-deep, deep and shallow *PACS* surveys at 75 , 110 and $170\ \mu\text{m}$ respectively.